Kaunas University of Technology

Faculty of Mechanical Engineering and Design

Design of Customized Unmanned Aerial Vehicle

Master's Final Degree Project

Konstantinos Loukas

Project author

Assoc. prof. Inga Skiedraite

Supervisor

Kaunas, 2021

Kaunas University of Technology

Faculty of Mechanical Engineering and Design

Design of Customized Unmanned Aerial Vehicle

Master's Final Degree Project

Mechatronics (6211EX017)

Konstantinos Loukas

Project author

Assoc. prof. Inga Skiedraite

Supervisor

Assoc. prof. Rūta Rimašauskienė

Reviewer

Kaunas, 2021

Kaunas University of Technology

Faculty of Mechanical Engineering and Design

Konstantinos Loukas

Design of Customized Unmanned Aerial Vehicle

Declaration of Academic Integrity

I confirm the following:

1. I have prepared the final degree project independently and honestly without any violations of the copyrights or other rights of others, following the provisions of the Law on Copyrights and Related Rights of the Republic of Lithuania, the Regulations on the Management and Transfer of Intellectual Property of Kaunas University of Technology (hereinafter – University) and the ethical requirements stipulated by the Code of Academic Ethics of the University;

2. All the data and research results provided in the final degree project are correct and obtained legally; none of the parts of this project are plagiarised from any printed or electronic sources; all the quotations and references provided in the text of the final degree project are indicated in the list of references;

3. I have not paid anyone any monetary funds for the final degree project or the parts thereof unless required by the law;

4. I understand that in the case of any discovery of the fact of dishonesty or violation of any rights of others, the academic penalties will be imposed on me under the procedure applied at the University; I will be expelled from the University and my final degree project can be submitted to the Office of the Ombudsperson for Academic Ethics and Procedures in the examination of a possible violation of academic ethics.

Konstantinos Loukas

Confirmed electronically

Kaunas University of Technology

Faculty of Mechanical Engineering and Design

Task of the Master's final degree project

Given to the student – Konstantinos Loukas

1. Title of the project

Design of Customized Unmanned Aerial Vehicle

(In English)

Bepiločio orlaivio, pritaikyto individualiems poreikiams, projektavimas

(In Lithuanian)

2. Aim and tasks of the project

Aim: To design customized drone with attached robotic manipulator for aerial manipulation and non-destructive testing.

Tasks:

1. To design improved drone frame and evaluate the severity of maximum payload on the drone during multiple flight states
2. To design and simulate a 4 DOF robotic manipulator attached on the drone
3. To calculate system characteristics (maximum payload, total flying time) and select system components (drone parts, robotic arm parts)
4. To calculate the cost of manufacturing the drone frame and robotic manipulator parts.

3. Initial data of the project

To adapt the previously proposed drone frame design and characteristics in order to be able to incorporate a functioning robotic manipulator.

4. Main requirements and conditions

Designing and system simulation via SolidWorks and Matlab. Prusa slicer will be used in order to simulate 3D printing of drone and robotic manipulator frames.

Project author	Konstantinos Loukas		
	(Name, Surname)	*(Signature)*	*(Date)*
Supervisor	Inga Skiedraite		
	(Name, Surname)	*(Signature)*	*(Date)*
Head of study field programs	Regita Bendikiene		
	(Name, Surname)	*(Signature)*	*(Date)*

Konstantinos Loukas. Design of Customized Unmanned Aerial Vehicle. Master's Final Degree Project, supervisor Assoc. prof. doc. Inga Skiedraite; Faculty of Mechanical Engineering and Design, Kaunas University of Technology.
Study field and area (study field group): Production and Manufacturing Engineering (E10), Engineering Sciences (E).

Keywords: NDT, UAV, FEA, Aerial Robotic Manipulator, Design, 3D Printing.

Kaunas, 2021. Number of pages 63.

Summary

There is a growing interest in the field of Aerial Manipulation systems where standard Unmanned Aerial Vehicles work in parallel with attached robotic manipulators in order to achieve tasks with the supervision or minimum supervision of the operating personnel. Such systems can be introduced in the field of Non-Destructive Testing and provide an alternative solution in monitoring the current state of systems and structures. This research project presents the design of a customized Unmanned Aerial Vehicle able to carry multiple payloads up to 3kg. The first chapter presents various Non-Destructive testing techniques and their implementation with Unmanned Aerial Vehicles. In the second chapter, a brief introduction on UAV's and the implementation of a compact customized system made for Aerial Thermography is presented. In the third chapter, an improved design was made in order to carry a fully functional 4 DOF manipulator. Firstly, the proposed design was tested via finite element analysis (FEA) in order to confirm the rigidity of the drone frame under various flight states and under maximum load carried by the drone. The results of the FEA presented sufficient rigidity during take-off, hovering, and pitch states. Then the components required for implementing the system were selected and the wiring diagram of the system is presented. The design and simulation of the robotic manipulator is presented next as well as the complete assembly of the proposed system. Finally, the cost of manufacturing the parts required for assembly of the UAV and robotic manipulator frames, as well as the cost of all electronic components, is calculated.

Konstantinos Loukas. Bepiločio orlaivio, pritaikyto individualiems poreikiams, projektavimas Magistro baigiamasis projektas, vadovė assoc. prof. doc. Inga Skiedraitė; Kauno technologijos universitetas, Mechanikos inžinerijos ir dizaino fakultetas. Studijų kryptis ir sritis (studijų krypčių grupė): Gamybos inžinerija (E10), Inžinerijos mokslai (E).
Reikšminiai žodžiai UAV, FEA, Dizainas.

Kaunas, 2021. Puslapių sk. p.63

Santrauka

Pastaruoju metu vis daugiau dėmesio yra skiriama ore valdomoms sistemoms, kur standartinės nepilotuojamos oro transporto priemonės dirba lygiagrečiai su pritvirtintais robotais manipuliatoriais, kad pasiektų jiems iškeltas užduotis esant pilnam ar dalinam jų valdymui. Tokio pobūdžio sistemos gali būti naudojamos neardomųjų bandymų srityje, kur jos gali pasitarnauti kaip alternatyvus sprendimas stebint ir įvertinant esamąją sistemų ir struktūrų būklę. Šiame darbe projektuojamas bepilotis orlaivis, pritaikytas individualiems poreikiams ir galintis gabenti kelis skirtingus krovinius iki 3 kg svorio. Pirmajame skyriuje pateikiami įvairūs neardomųjų bandymų metodai ir jų įgyvendinimas naudojant bepiločius orlaivius. Antrajame skyriuje pateikiama trumpa apžvalga apie bepiločius orlaivius bei pristatoma sukurta kompaktiška sistema oro termografijai. Trečiajame skyriuje pristatomas patobulinta konstrukcija, pritaikyta veikiančiam keturių laisvės laipsnių roboto manipuliatoriaus gabenimui. Pirmiausia siūloma konstrukcija buvo išbandyta baigtinių elementų metodu (BEM), siekiant patvirtinti orlaivio rėmo tvirtumą esant skirtingoms skrydžio metu būsenoms ir didžiausiai orlaivio apkrovai. Baigtinių elementų metodo rezultatai parodė tvirtumą pakilimo, kybojimo ir tangažo būsenose. Toliau pateikiama informacija apie reikiamų komponentų pasirinkimą bei pristatoma sistemos pajungimo schema. Taip pat pateikiami roboto manipuliatoriaus konstrukcija bei modeliavimo rezultatai kartu su pilna visos sistemos surinkimo informacija. Pabaigoje apskaičiuojamos komponentų reikalingų bepiločio orlaivio ir roboto manipuliatoriaus konstrukcijoms integruoti išlaidos kartu su elektroninių komponentų išlaidomis.

Table of contents

List of figures

List of tables

Introduction

The fourth industrial revolution or Industry 4.0 has introduced numerous technological advancements that are currently allowing manufacturers to achieve new levels of continuously undisrupted production. Nevertheless, such manufacturing achievements directly affect the prevailing maintenance standards and requirements and calls for new and improved methodology. When it comes to predictive maintenance techniques, manufactures found themselves in need of advancing the existing methodology of Non-Destructive Testing [1,2,3] in order to ensure that their maintenance schedules incorporate fast and less complicated prediction methods guaranteeing good operation of the used equipment. Moreover, the need of autonomous or semiautonomous testing with the use of Unmanned Aerial Vehicles (UAV's) seems a prominent field in which many investigations and research projects [4 – 9] have been conducted, since UAV's have the ability to reach hazardous environments or contaminated areas without putting in danger the operating personnel. Furthermore, recent global pandemic brought restrictions, which limit or even deny human contact, making the task of using contact type testing methods even more difficult to implement. Therefore, the possibility of integrating NDT equipment into Unmanned Aerial Vehicles is a feasible solution offering various advantages to the end user, while integration of robotic manipulators assisting in performing contact type testing into customized UAV's can further support the resolution of the above-mentioned contact type testing issues.

The primary goal of this project is to design a customized aerial vehicle assembling printable components and modifiable according to the requirements of the given task. The designed system should be able to incorporate an aerial manipulator, which can introduce additional options to the designed system. The required components as well as the total cost of this custom build is minimized in order to make the system financially viable.

Aim and tasks of the project:

Aim: To design customized drone with attached robotic manipulator for aerial manipulation and non-destructive testing.
Tasks:

1. To design improved drone frame and evaluate the severity of maximum payload on the drone during multiple flight states
2. To design and simulate a 4 DOF robotic manipulator attached on the drone
3. To calculate system characteristics (maximum payload, total flying time) and select system components (drone parts, robotic arm parts)
4. To calculate the cost of manufacturing the drone frame and robotic manipulator parts.

1. Non-destructive testing

Non-Destructive Evaluation (NDE) or Non-Destructive Testing (NDT), is the field of science which includes the characterization and identification of defects on the surface or interior of different materials without altering their characteristics and morphology or damaging the materials under testing. By performing NDT, the user can evaluate the condition of the materials or components in comparison with some predefined standards. By doing so, the given state of a material, machine component, building or structure can be defined. NDT is a cost-effective way to predict possibly breakdowns which can have both social and commercial impact [1].

In order to perform NDT, the user must be acquainted with the material specifications and characteristics since different material requires different type of testing. In many cases defect finding, and proper identification require the application of more than one NDT technique in order to correctly characterize and identify the type and severity of the problem [2]. Comparing to traditional distractive testing techniques where the material under testing is altered or damaged permanently, NDT techniques are suitable for use in various fields such as quality inspections and control, military and defense, power plants, aerospace, construction sites, automotive and other manufacturing industries.

In general NDT techniques can be divided into two major categories. Contact based testing methods and contact-less testing methods. Each category offers a wide range of testing techniques suitable for different applications. Table 1 presents the most common methods used under these categories.

Table 1. Contact and Contactless NDT techniques [3]

Contact NDT	Ultrasonic testing, Eddy current testing, Magnetic & Electromagnetic testing, Penetrant & Liquid penetrant testing
Contact-less NDT	Through transmission Ultrasonic testing, Radiography, Thermography & Infrared testing, Holography, Shearography, and visual testing

1.1. Integration and automatization of NDT

NDT techniques are useful tools which can provide valuable information's about the current state of a system or components of a system. Normally NDT techniques are performed by maintenance personnel who are responsible for the operation and good performance of a system or a structure. Any of the mentioned NDT methods can be included in preventive or predictive maintenance schedules and performed periodically in order to avoid major setbacks and breakdowns which could lead to production losses or safety and environmental breaches.

The continuous monitoring of such systems can be a tedious task which requires well trained personnel with knowledge of the system and the applied NDT method. In many cases the application of NDT requires time consuming preparations and specialized personnel which can access the equipment under testing. For example, customized scaffolding, ropes, and ladders are used in order to perform testing in equipment which are on height. Such methods can put the life of the personnel performing the testing in danger. The need of a safer, reliable, and faster way of performing NDT has led to the development of systems which can be integrated into Unmanned Aerial Vehicles (UAV's). Such systems require minimum time of preparation and deployment, can cover larger areas in less time and can be customized to the need of the application under testing.

1.2. NDT applications via flying drones

Tsanakas et all [4], made use of a thermal camera attached to a Condor AY 704 UAV, in order to perform thermographic inspection of photovoltaic panels. The team took thermal pictures also called thermographs, to detect faults such as hot-spots, fractured cells, disconnected arrays, or other dirty spots which affect the total performance of the system. These pictures were used by the team in order to create a thermal map by using aerial-triangulation and terrestrial georeferencing methods. Faulty spots are marked with different colors on the map which makes it easier to understand, locate, and correct them. Tarek Omar et all [5], used a similar system in order to perform thermographic inspection on two reinforced concrete bridge decks. They made use of thermographs taken by a thermal camera attached to a drone in order to locate subsurface delamination areas. In this case the pictures were stitched together by Matlab algorithm which can identify identical pixels on the edges of each thermograph and connect them together in order to produce a thermal map of the area. Areas on the map where delamination issues are present, tend to present higher temperature than other neighboring spots. In both presented cases aerial thermography was used which is part of the Non-contact NDT methods, L.M. Gonzalez-deSantos et all [6], created a system which consists of an ultrasound sensor attached to a drone in order to contact ultrasound thickness testing of metal sheets. Ultrasound testing is a contact type NDT method. In this case, the attached sensor must establish clear contact with the surface under testing. To do so, the team made a custom-made 3D printed contact support where two Lidar distance sensors were attached and used in order to calculate the distance and angles between the drone and the metal surface under testing. Custom control algorithms were created in order to achieve the desired drone control during the measurement process. A similar research was presented by Basaran Bahadir Kocer et all [7], where an ultrasonic Bluetooth sensor was placed on a custom-made compression mechanism on the top of a quadcopter. This system uses the feedback signal from the spring compression mechanism in order to maintain steady contact with the surface under testing. The system was used for thickness measuring of acrylic ceiling. The team intends to use the proposed system for ceiling thickness measurement inside tunnels. Marco Tognon et all [8], contacted welding condition inspection by using the eddy current contact NDT method. They used a drone system equipped with an eddy current controller and its probe in order to inspect the welding condition of a metal piping system. A custom-made 3D printed arm with 2 DOFs was used to attach the probe pen on the drone. The team created a weldment map by taking measurements via push and slide inspection on the surface of the pipe. By doing so possible flaws or cracks on the welded area could be detected. Anibal Ollero et all [9], presented an article which summarizes new developments of aerial robotic manipulators applied for outdoor industrial inspections and maintenance. The AEROARMS project as it is known, presents three different cases where a UAV equipped with a robotic manipulator was used in order to achieve the given task. Direct contact measurements, deployment of robotic crawlers and sensors installation via dual-arm manipulators was possible with the use of multirotor aerial vehicles equipped with lidars, stereo cameras, optical flow sensors, and other inertial measuring units.

In this chapter, a classification of NDT methods, their importance, possibilities of integration and automatization via flying drones was presented. All mentioned projects make use of commonly available commercial drones which have been customized with appropriate attachments in order to perform the NDT task in hand. The classification, characteristics, and design of a customized aerial vehicle with 3D printed custom parts and a selection of electronic components is presented on the next chapter.

2. Unmanned aerial vehicles

The term UAV describes all types of unmanned aircrafts able to perform autonomous or semi-autonomous flights. During flight, all settings are controlled by specialized pilots located in ground stations or are preloaded into the drone's internal system. Drones have been used for many applications and in many different fields such as photography and cinematography, surveillance and military, mapping, wildlife monitoring and historical conservation, search and rescue missions, delivery of goods, monitoring of infrastructures and other inspections.

UAV's can be classified according to [10]:

- Operation level: low, medium, high, or very high altitude
- Size: micro / nano, small, medium, or large
- Flight endurance: low up to 30min, medium 30 to 60min, long more than 60min
- Weight: light less than 2kg, medium 2-5kg, heavy above 5kg
- Wing type: fixed wing, rotary wing, hybrid wing
- Autonomy level: human operated - manual control, human delegated - semi-autonomous, human supervised - autonomous based on predefined settings, and fully autonomous
- Power source used: battery type, solar energy, kerosene, or other oil type fuels.

2.1. Quadcopters

One of the most common UAV systems is a quadcopter. A quadcopter is rotary wing type UAV which makes use of DC motors attached to its body in order to produce lifting force. Propellers arranged in pairs, two rotate clockwise (pullers) and two counterclockwise (pushers), are attached to the DC motors of a Quadcopter. The size and shape of the propeller depends on the design and application used. Motor speed adjustments create the necessary thrust, torque and direction which are equivalent to the yaw, pitch, and roll angles. [11]. Fig. 1 shows the outcome of the speed adjustments and Fig. 2, the acting forces ($F1 - F4$ and weight), angular speeds ($\omega 1 - \omega 4$), and the pitch, roll, and yaw angles in relation to the world frame.

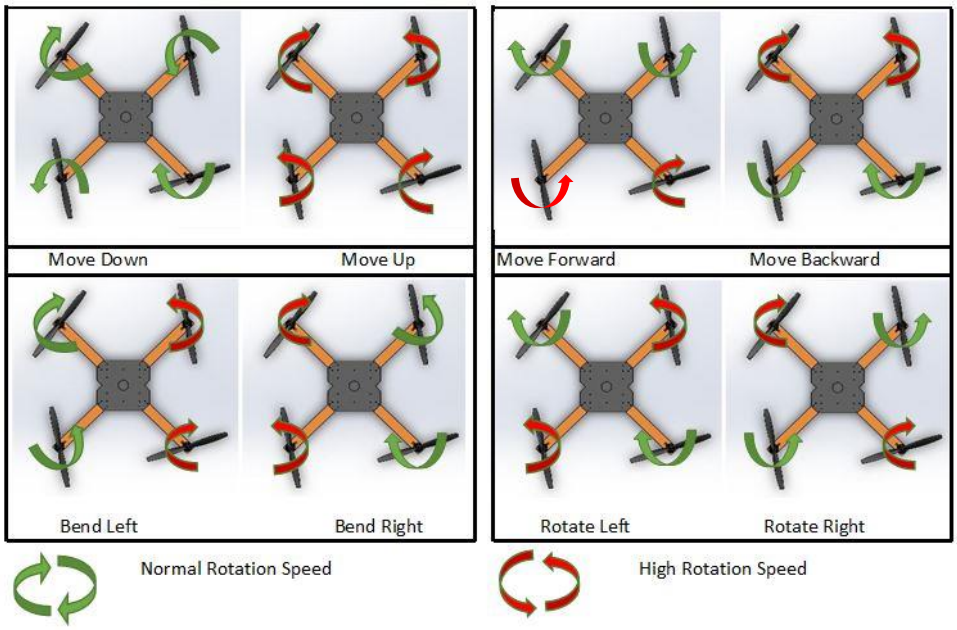

Fig. 1. Realized control by motor speed changes, design made in Solidworks

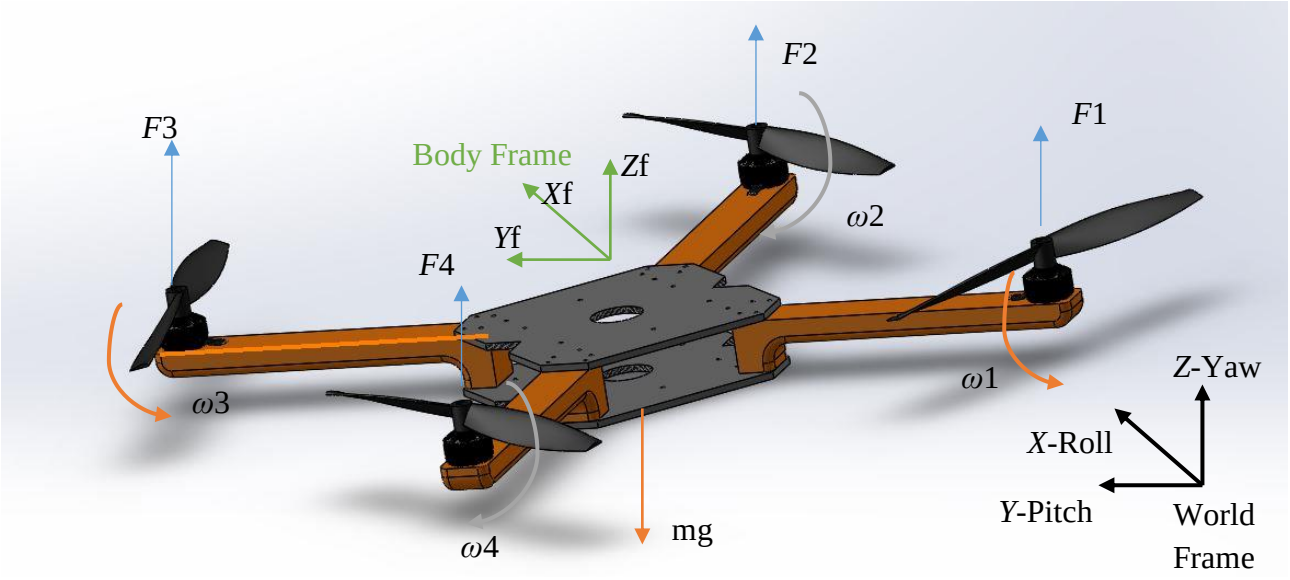

Fig. 2. Acting forces and system of coordinate of a quadrotor UAV, design made in Solidworks

2.2. Guidance, navigation, and control methods

Several methodologies for drone control and navigation have been implemented. Guidance, Navigation, and Control or GNC of UAV's can be achieved by radio or video control or by an autopilot system. In radio communication, control of the drone is realized through electromagnetic waves transmitted by a controller and received by a paired receiver attached to the body of the drone. The received signals are converted into commands by a flight controller (FLC), which is responsible for transferring those commands to the electronic speed controllers (ESC's) controlling the DC motors. Similarly, video communication systems can transmit live image or record videos and photographs and transmit them through specialized video transmitters to ground monitors. The user then can control the drone according to the image captured by the camera installed on the drone. Presently, advanced monitoring and surveillance systems can carry thermal, infrared, or night vision cameras to accomplish different tasks.

Another common UAV control method is through autopilot systems. In this case the drone can plan and navigate autonomously though preloaded flight plans. Also, data collected by the drone's internal systems can be transmitted into ground stations where they are analyzed by ground computers and transmitted back to the drone's flight controller. These instructions are used in order to alter the flight plan accordingly [12].

2.3. Drone system design for aerial thermography

A compact quadrotor drone was designed in order to perform aerial thermography [13]. The main characteristic of the customized drone was its compact 3D printable frame. The design was able to sustain total 1kg of load mounted on the middle of the drone frame. Static finite element analysis was performed in Solidworks simulations in order to verify this assumption. The cost of manufacturing the drone frame was calculated at 12.58 Eur. The customized drone can be seen in Fig. 3. and Fig. 4.

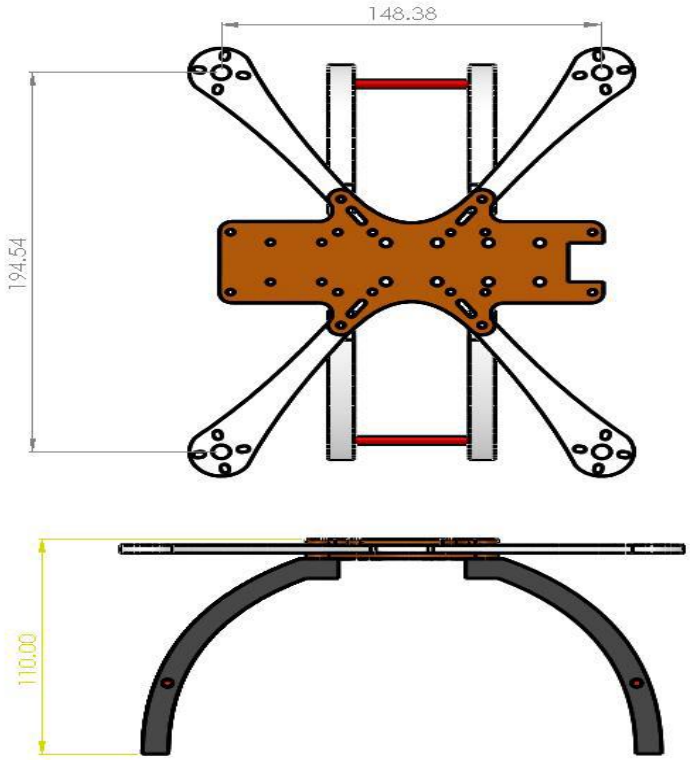

Fig. 3. Solidworks design of drone frame made for aerial thermography

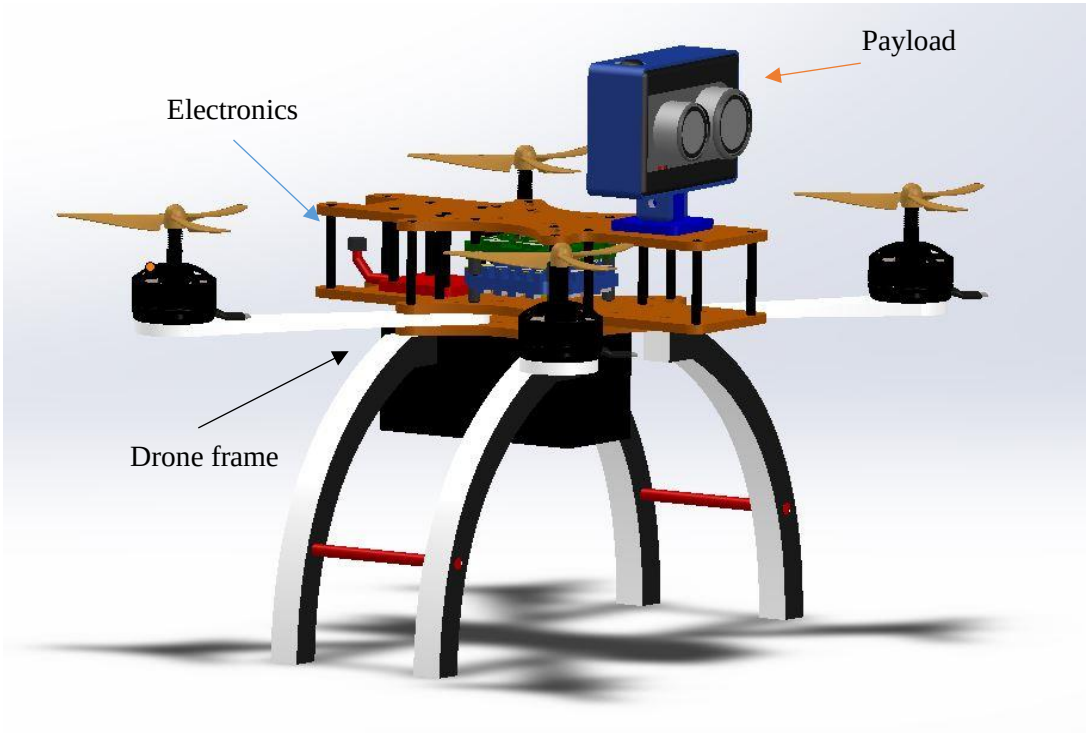

Fig. 4. Solidworks design of compact drone with attached thermal camera

The main components used for the proposed system can be divided into three categories.

- Drone frame
- Electronics
- Payloads

2.3.1. Drone frame design for aerial thermography

The design of the frame and the static analysis was performed in Solidworks, where two different materials, ABS filament and Carbon enhanced ABS filament investigated in order to determine if an enhanced material can improve the mechanical characteristics of the frame. The simulation presented slightly improved results under static nodal stress for the carbon enhanced ABS filament (0.290 MPa vs 0.306 MPa). Table 2 presents the results of the static analysis.

Table 2. Static analysis results of the proposed frame under 1kg of total load

Method	ABS Filament	Carbon Enhanced ABS Filament
Max. Nodal stresses	0.306 MPa max	0.290 MPa max
Max. Displacement	0.031 mm	0.037mm
Max. Strains	0.0001	0.0001

Then the total cost of 3D printing the frame components was calculated. For the calculations three different set of 3D printing settings were considered. The results of the comparison found cheaper option for the parts made of ABS filament. Although the difference with the Carbon enhanced ABS filament for the same settings was very small. Table 3 presents the results of the cost calculation.

Table 3. 3D printing cost in Eur for compact drone frame

SN	ABS Filament	Carbon Enhanced ABS Filament
1	12.58	14.80
2	13.09	15.82
3	13.77	17.18

2.3.2. Drone electronics selection for aerial thermography

The proposed system is combined by a selection of electronic components put together a shown in Fig. 5. These components can be bought separately and interchanged by similar components. This is an advantage since the need for spare parts or upgrades on the system is relatively easy and can be adjusted as per the requirement of the task in hand. A list of the selected components is shown on Table 4. Drone electronics for aerial thermography.

Table 4. Drone electronics for aerial thermography [14]

Part Name	Part Description	Model 1	Price in Euros
Drone frame	Main drone frame, 3D printed	Custom Print	12.58
Motors	To provide trust for drone	Emax 2750 kv	89.4
Propellers	To attach to DC motors	5045	5
ESC	Electronic speed controller to control motors speed	Tekko32 by Holybro	104
Flight Controller	Flight controller to translate received signals and communicate to ESC for motor speed adjustments	Kakute F7 by Holybro	

Receiver	To receive control commands from ground transmitter	FrSky XM Micro by FrSky	18.45
Transmitter	To control the drone	Taranis X9 Lite by FrSky	117.43
Video transmitter	Video transmitter to broadcast live image to ground receiver	VTX Rush Tank mini and Cherry RHCP antenna by RushFPV	64
LiPo Battery	To power up the system	LiPo Zop Power 5000mAh 4Cell	44.8
Battery charger	To re-charge the battery	Imax B6 50W	35
Total			490.66

The total amount of this project comes to 490.66 Eur, this cost does not include the cost of the thermal camera. The selection of the components can be optimized according to the requirements of the user. For example, the total flight time can be increased by using battery with more capacity or by using motors with higher ratings in terms of produced power.

The components of the system are wired together as soon in Fig. 5. The four motors of the system are connected to the electronic speed controller via three wires, one for each face. The rotation of the motors can easily be altered by interchanging any two wires. Power is transmitted to the flight controller through the speed controller via the 5V port, also four signal wires are connecting the motors to the flight controller via the speed controller. Finally, the receiver, GPS sensor and video transmitter are connected with the flight controller. Each module requires 5V and ground connection and returns signals through RX and TX ports.

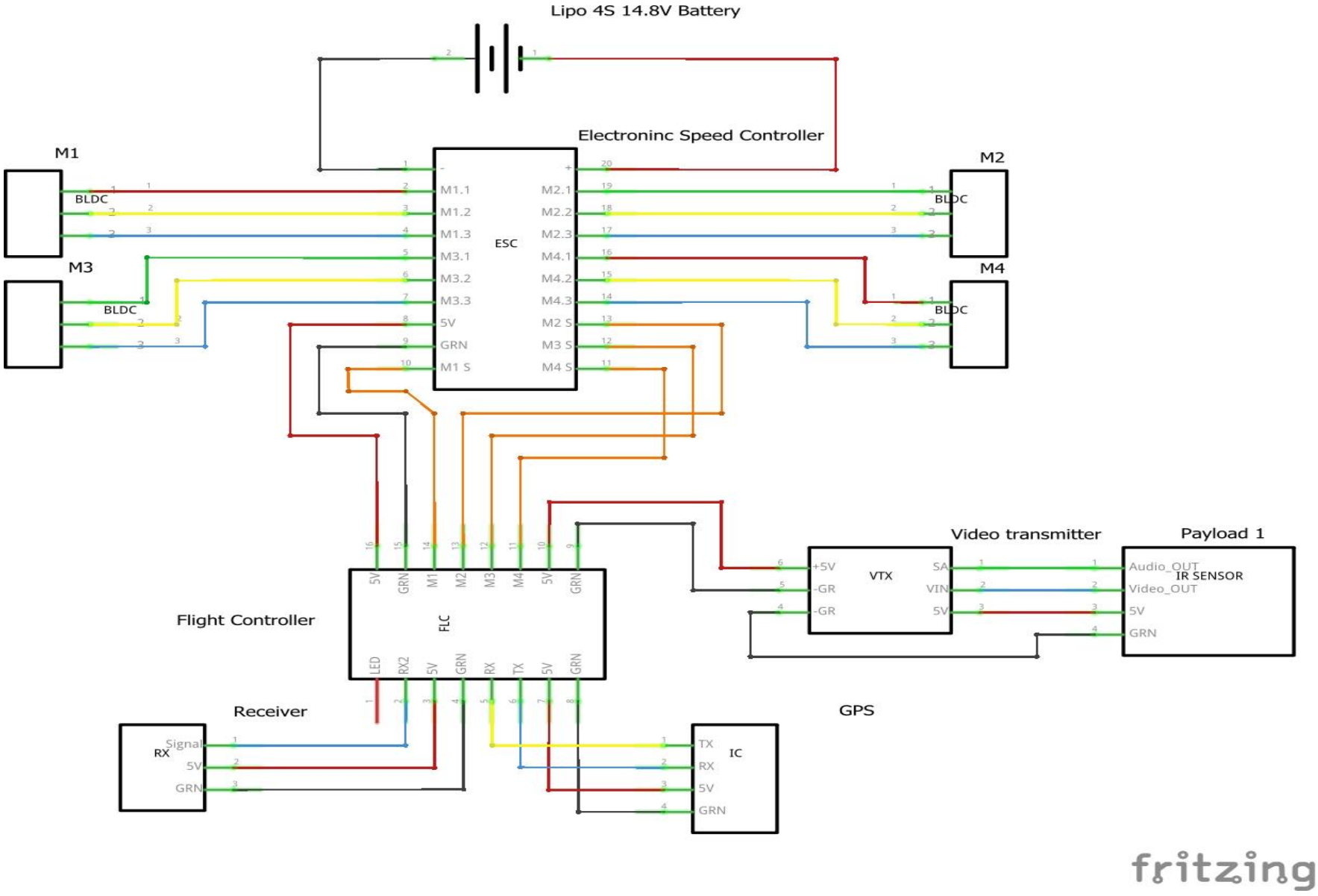

Fig. 5. Wiring diagram of proposed system made for thermography, made in Fritzing

2.3.3. Drone payload selection for aerial thermography

The term payload describes any supplementary equipment attached to the drone system. The qualities of the payload identify the main purpose and capacities of the system. In this case, a Flir duo camera was selected in order to perform photogrammetry and thermography inspection and condition evaluation of different kind of structures or materials. This camera features a combination of two lenses, a standard RGB 4mm, f/2.8, 4K Pixel lens and a 13mm 640 x 512 Pixel infrared sensor. The user can choose which sensor is active for recording at any given time.

Photogrammetry is the area of science which includes analysis of photographs by various methods in order to extract valuable information's about an object and its environment. Similarly, the term thermography describes the technique of capturing low wavelength (3μm – 14μm), infrared radiation images consist of different colors representing the different temperatures on an object, structure, or material. Such images are known as thermographs [15].

The success of a thermographic inspection is related with the quality of the captured thermographs. Resolution, thermal sensitivity, and accuracy are three main factors affecting the quality of the study. Thermal detectors with high resolution can provide images with higher number of pixels present on a captured image. The sensitivity and accuracy of a thermal detector can be affected by the type of the infrared detector. Cooled and uncooled infrared detectors are the most common detector types available in the market currently. Cooled type detectors have minimum influence from the ambient temperature on the final measurement since they are placed in vacuum sealed cooled type cases thus, they offer better results in comparison with the uncooled type detectors [16].

Various types of thermal cameras are currently available in the market, though not all are suitable for implementation of aerial thermographic systems. The size of the camera is a catalytic factor in the design of an aerial system. Compact, lightweight cameras such as those presented on Table 5, are easier to intergrade and control on UAV's.

Table 5. Thermal cameras for aerial thermography [17, 18, 19]

Manufacturer	Name	Resolution	Price (Euros)
Flir	Duo Pro R	4k RGB sensor & 640x512 IR sensor	4348
Flir	Vue Pro R	336x256 RGB & 640x512 IR	2800
Flir	Vue Pro	336x256 RGB & 640x512 IR	1964
Flir	Lepton	80x60 IR sensor	649
Workwell	Wiris Pro	1920x1080 RGB & 640x512 IR	17000
Workwell	Wiris 2^{ND} GEN	640x512 IR sensor	9295
Workwell	Wiris Mini	1600x1200 RGB & 384x288 IR	4000
Yuneec	CGOET	160x120 IR sensor	1589
Yuneec	E10T	336x256 RGB & 640x512 IR	6690

Table 5 presents thermal cameras currently available on the market which are used for aerial thermography. The cost of the camera depends mostly on the resolution of the thermal sensor, simple thermal sensors are available as from 649 Eur while high end models cost up to 17.000 Eur.

3. Design of improved system with enhanced capabilities

The quadcopter drone designed for aerial thermography presented in the previous chapter, is characterized by its compact design, 3D printed frame, and ability to perform long lasting inspections due to its lightweight structure. The weight of the whole system was calculated at 850grams and the total flight time with a fully charged battery was estimated to 35 minutes. Although the design seems suitable for the selected application its limited to smaller and lighter payloads due to its compact design. Moreover, the drone frame rigidity was checked only by static finite element analysis, leaving unknown the impact of dynamical forces acting on the drone during flight. Also, the cost of the electronic components totals to 490.66 Eur without the cost of the thermal camera. A new customized design featuring a more durable construction able to carry heavier payloads and the selection cheaper electronic components with lower cost but with the same characteristics is presented on the following chapter.

3.1. Quadcopter frame

In order to optimize the frame of the quadcopter designed for aerial thermography, its necessary to predefine the requirements which the new frame design has to fulfill. The new frame design should be able to carry the weight of all the electronic components and attached payloads and also extra load which will be later applied on the drone. The amount of the extra load will be defined according to the maximum load which the structure can safely carry and the maximum thrust which the selected motors can provide in order to lift the weight of the drone. To verify the design, non-linear dynamic nodal stress analysis and impact analysis will be performed on Solidworks where boundary conditions such as gravity, weight, and lift forces are applied.

The design of the new frame is based on the number of actuators used to produce lifting force which is required in order to make the drone fly. Also, the size of the propellers is very important since larger propellers require longer wings to avoid collisions between them during operation. The center of gravity or COG, of the system is another factor which affects the stability of the drone during flight [20]. All components must be firmly placed as closer as possible to the center of balance in order to avoid excessive movements of the drone during hovering mode.

A quadcopter ‘X’ type design is chosen for this project featuring four actuators placed in a way that the shape of the model looks like the alphabetic letter X, the size of the arms is adjusted in order to combine 10-inch propellers. The design of the new frame will be done in Solidworks and printed on Prusa i3 MK3 3D printer, also ABS filament was chosen as the main material for the drone frame since the cost versus the advanced mechanical properties which other carbon enhanced ABS filaments offer does not justify their selection [13].

3.1.1. Design of improved frame

In order to accommodate larger propellers, the wingspan of the quadrotor was increased, although by increasing the size of the parts the total time, material used and cost for 3D printing the drone frame will change accordingly. With these in mind the following parts were created and shown in Fig. 6 and Appendix 1. Technical drawings.

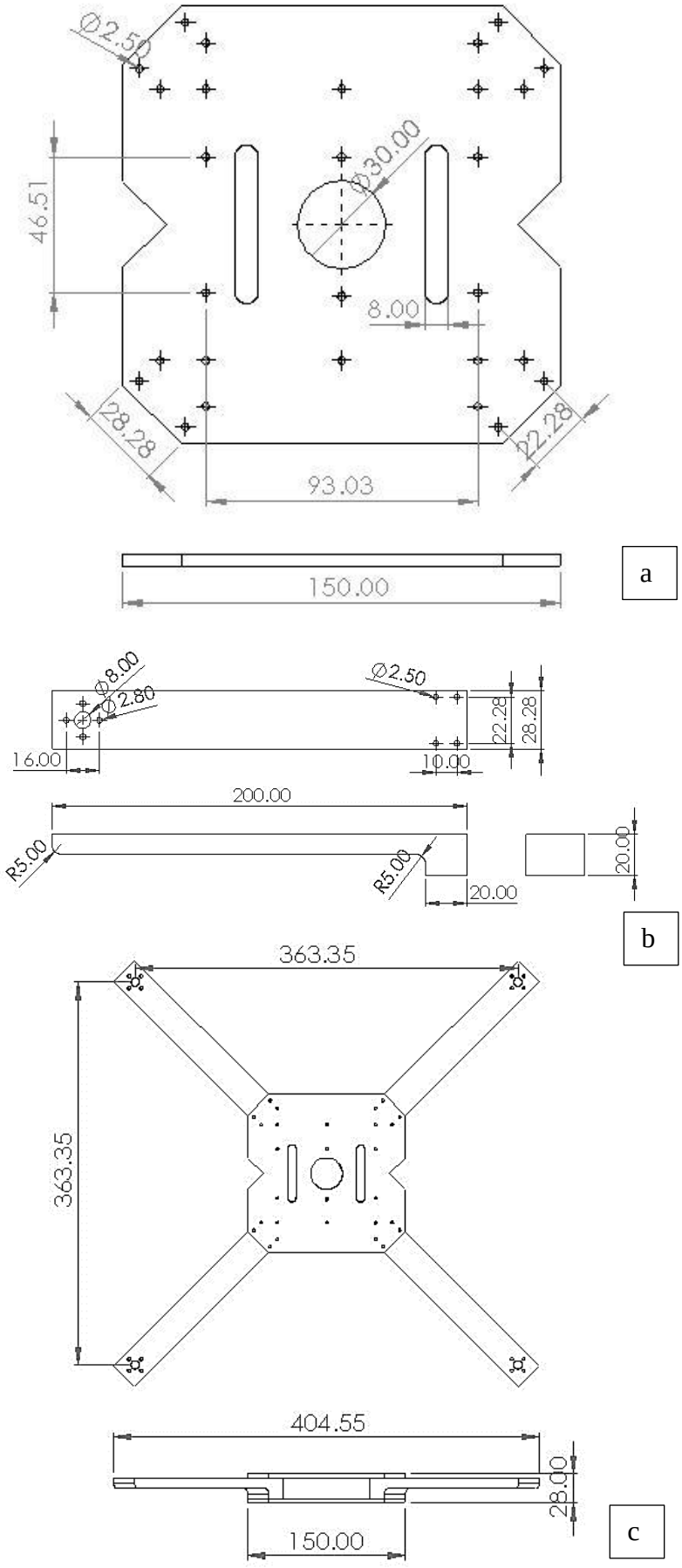

Fig. 6. Parts of improved drone frame, design in Solidworks: a) Frame plates b) Wings c) Assembly view

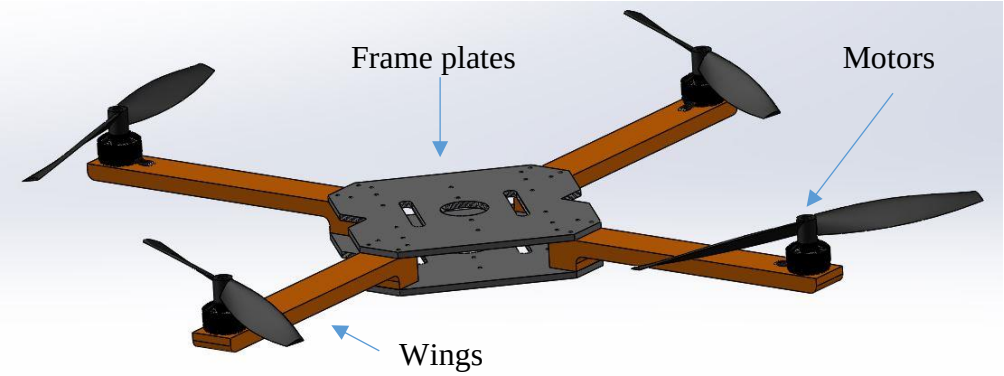

Fig. 7. Solidworks assembly view of improved design, main body, wings, and motors

The drone frame consists of two base plates and four wings which are held together by hex head 3mm screws. At the end of each wing are attached the motors with their propellers. The rest of the electronic components will be mounted on the center of the frame.

3.1.2. Frame finite element analysis

The rigidity of the new frame was tested for several flight conditions by finite element analysis on Solidworks. As material a custom ABS material was created whose mechanical properties can be seen on Table 6. To simulate different flight stages, the total weight of the drone system as well as the maximum thrust produced by the propeller's must be known.

The selected set of motors and propellers along with a three cell lipo battery, can provide maximum 860g of thrust force per motor. With this in mind, the total lift force which the drone can provide equals to 3.44 kg.

Table 6. Easy ABS filament mechanical properties [21]

Property	Value	Units	Test Method
Tensile Modulus	2140	N/mm^2	ISO 527-2
Tensile Stress (Yield 3.2mm), Injection Molded	43	N/mm^2	ISO 527-2/50
Tensile Strain	2.7%		ISO 527-2/50
Flexural Modulus	2050	MPa	ISO 178[1,2]
Flexural Strength	65	MPa	ISO 178[1,2]
Mass Density	1050	kg/m^3	ISO 1183/B
Heat Deflection Temperature	101	°C	ISO 75-2/A

The mechanical properties of the ABS thermoplastic material are based on the properties provided by the manufacturer of the filament, although the mechanical properties of FDM printed parts can be affected by printing settings such as the temperature of the extruder, layer height, printing speed and inter-layer bonds [22]. For these reasons, the safety factor of the design should be kept heigh.

1. Take-off mode simulation

The first test simulates the forces acting on the quadcopter frame during take-off mode. In order to have a successful take-off the lift forces produced by the propellers of the drone must overcome the

gravity and the total weight of the drone system. The forces used for this simulation can be seen in Fig.8, and the results of the simulation in Fig. 9, and Fig. 10.

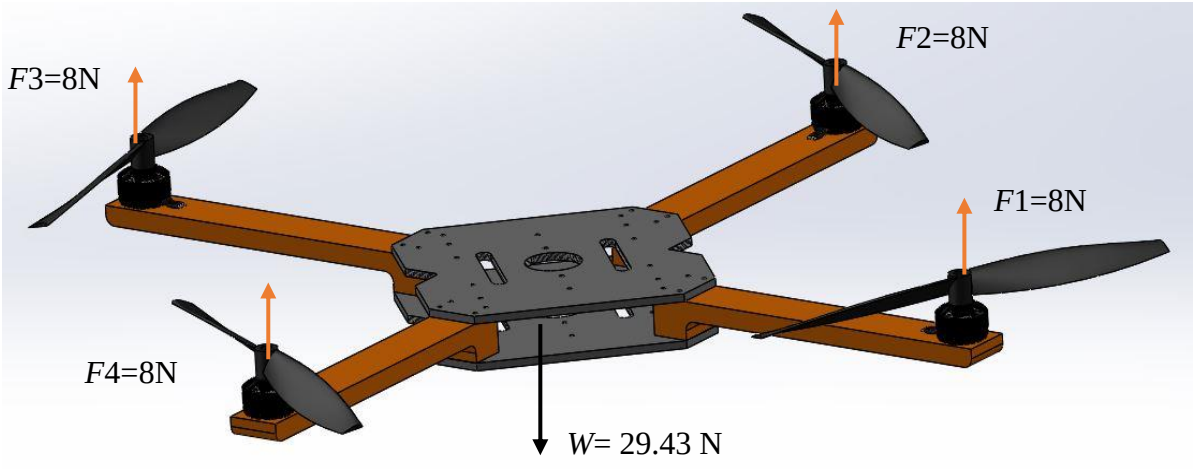

Fig. 8. Forces acting of the quadcopter during take-off

Simulation initial settings and results: Materials used = ABS custom filament, Connectors: Hex 3mm SS bolts with nuts, Fixtures: Connecting points, External Loads: Vertical force of weight W=29.43 N, Lifting forces on each motor $F_{1\text{-}4}$= 8N.

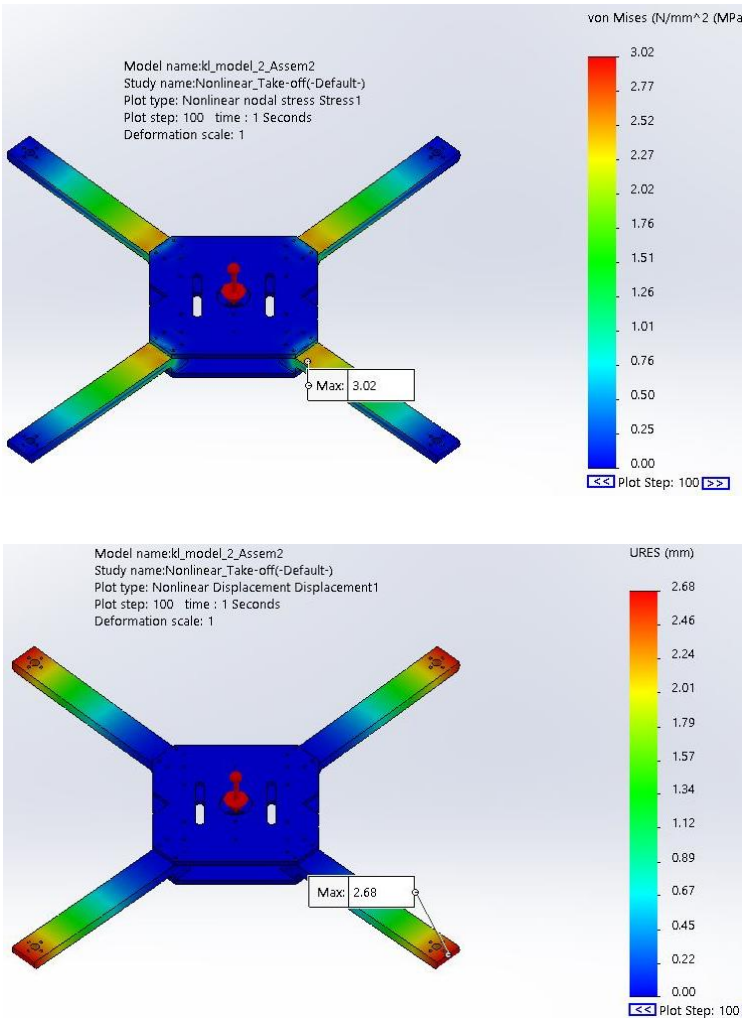

Fig. 9. Stress (a) and displacement (b) plots during take-off

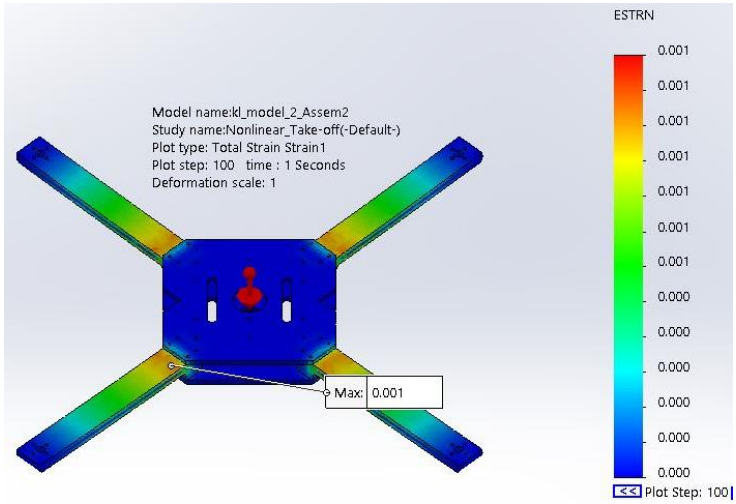

Fig. 10. Strains plot during take-off

It was observed that the maximum stress forces of 3.02MPa, appeared between the connections of the wings and the main frame plates. Also, the maximum displacements 2.66mm, observed at the edge of the wings where the motors are attached, minimum strains appeared also between the wings and the main body.

2. Hovering mode simulation

The second test simulates the forces acting on the quadcopter frame during hovering mode. Hovering state is achieved when then quadcopter has accomplished successful take-off and is now holding a stable position above the ground. In this case the lifting forces provided by the drone's actuators are matching the weight of the drone. The forces used for this simulation can be seen in Fig.11, and the results of the simulation in Fig. 12.

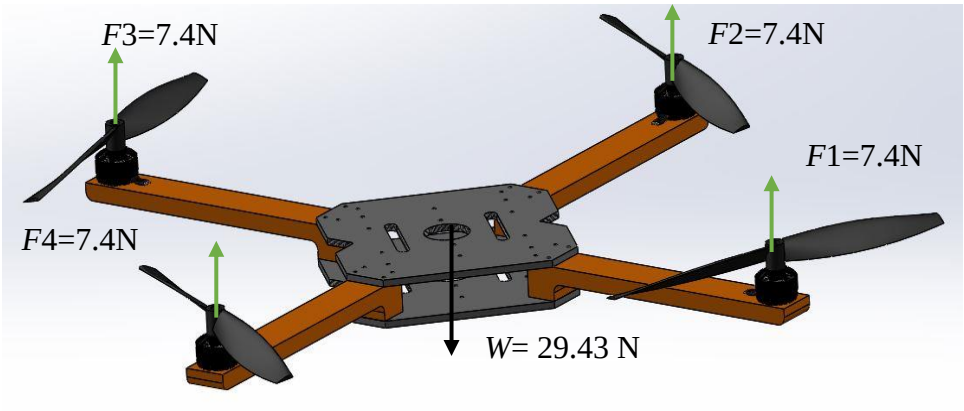

Fig. 11. Forces acting of the quadcopter during hovering

Simulation initial settings and results: Materials used = ABS custom filament, Connectors: Hex 3mm SS bolts with nuts, Fixtures: Connecting points, External Loads: Vertical force of weight W=29.43 N, Lifting forces on each motor $F_{1\text{-}4}$= 7.4N.

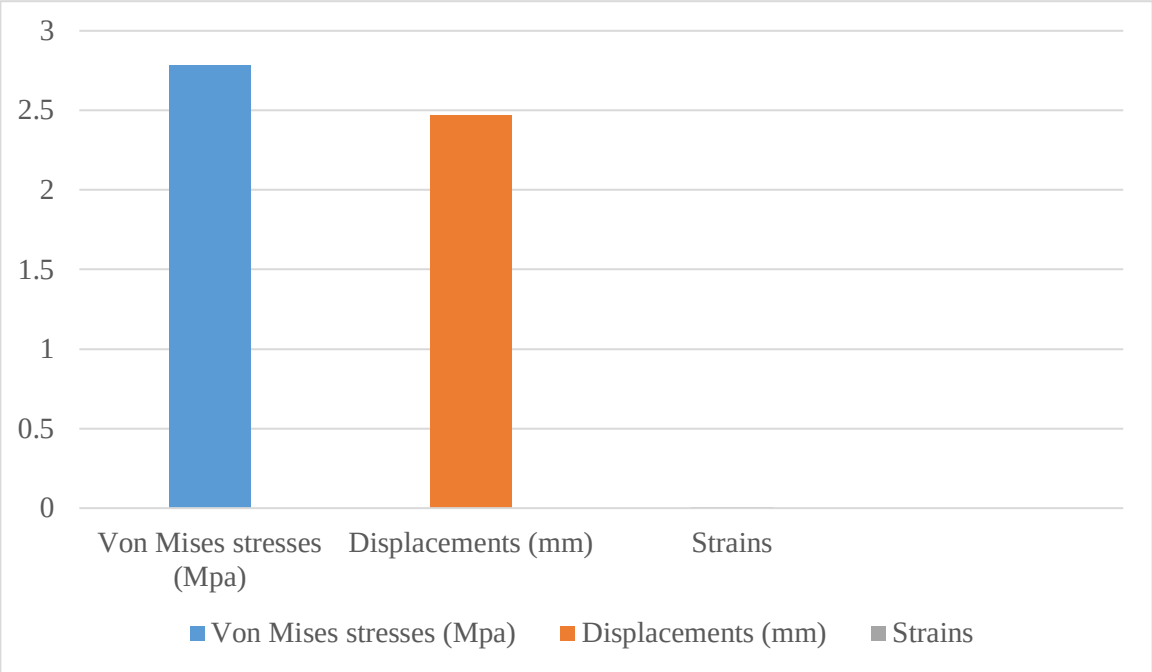

Fig. 12. Hovering state simulation results

It was observed that during hovering state the maximum stress forces of 2.78MPa, appeared between the connections of the wings and the main frame plates. Also, the maximum displacements 2.47mm, observed at the edge of the wings where the motors are attached, minimum strains appeared also between the wings and the main body.

3. Moving forward (pitch) mode simulation

This test simulates the forces acting on the quadcopter frame during any kind of pitch motion. In this case the adjustment of motor's speed varies between the front motors and the back. In order to realize forward movement, the back motors must rotate faster than the front motors of the drone. The forces used for this simulation can be seen in Fig.13, and the results of the simulation in Fig. 14.

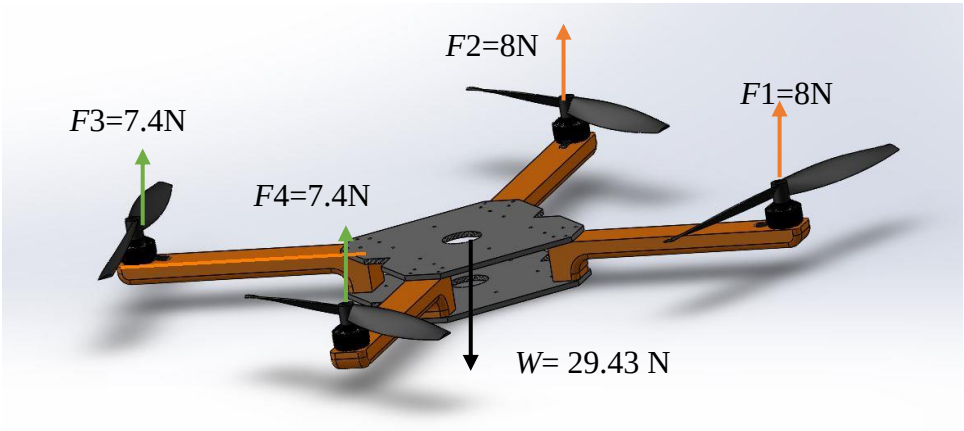

Fig. 13. Forces acting of the quadcopter during pitch state

Simulation initial settings and results: Materials used = ABS custom filament, Connectors: Hex 3mm SS bolts with nuts, Fixtures: Connecting points, External Loads: Vertical force of weight W=29.43 N, Lifting forces on each motor $F_{1\&2}$= 8N, $F_{3\&4}$= 7.4N

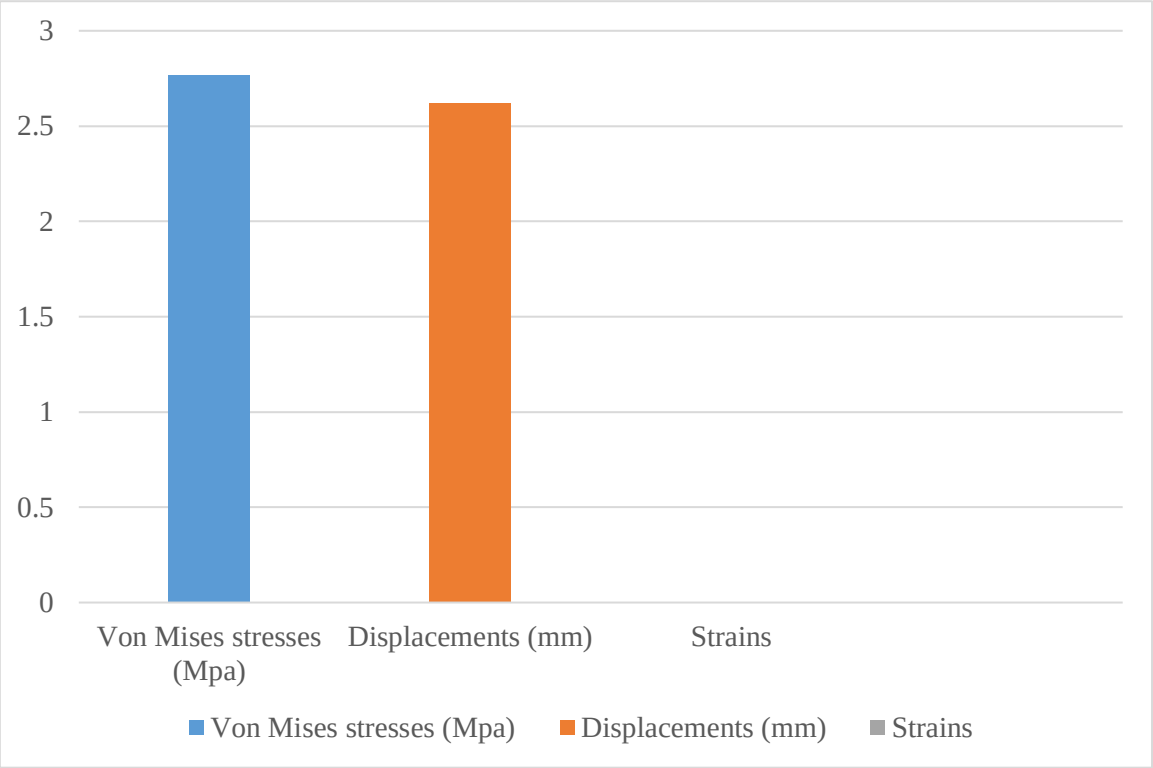

Fig. 14. Simulation results during forward pitch motion

It was observed that during pitch state the maximum stress forces of 2.77MPa, appeared between the connections of the wings and the frame pieces. Also, the maximum displacements 2.62mm, observed at the edge of the wings where the motors are attached, minimum strains appeared also between the wings and the main body.

4. Drop test analysis

The last FEA simulates the effect of impact of the quadcopter frame with the ground or any other object during flight. Drop test study is another non-linear study which is included in Solidworks simulation platform. There are two major sub-categories of this study. Drop test from predefined height, and velocity during the impact study. In drop test 1, is simulated the fall of the quadcopter from 3 m height. Such condition can be created in case of an unforeseen failure on the system. The second drop test simulates the impact of the quadcopter with an object during fly. The forces acting on the frame of the quadcopter for drop test 1 and 2 and the results of the simulations can be seen on Fig. 15 to Fig 18.

- **Drop test 1**

  Initial settings: Drop from height = 3m, Gravity 9.81 m/sec^2, Target is normal to gravity, Rigid tarter, Contact damping = 1.

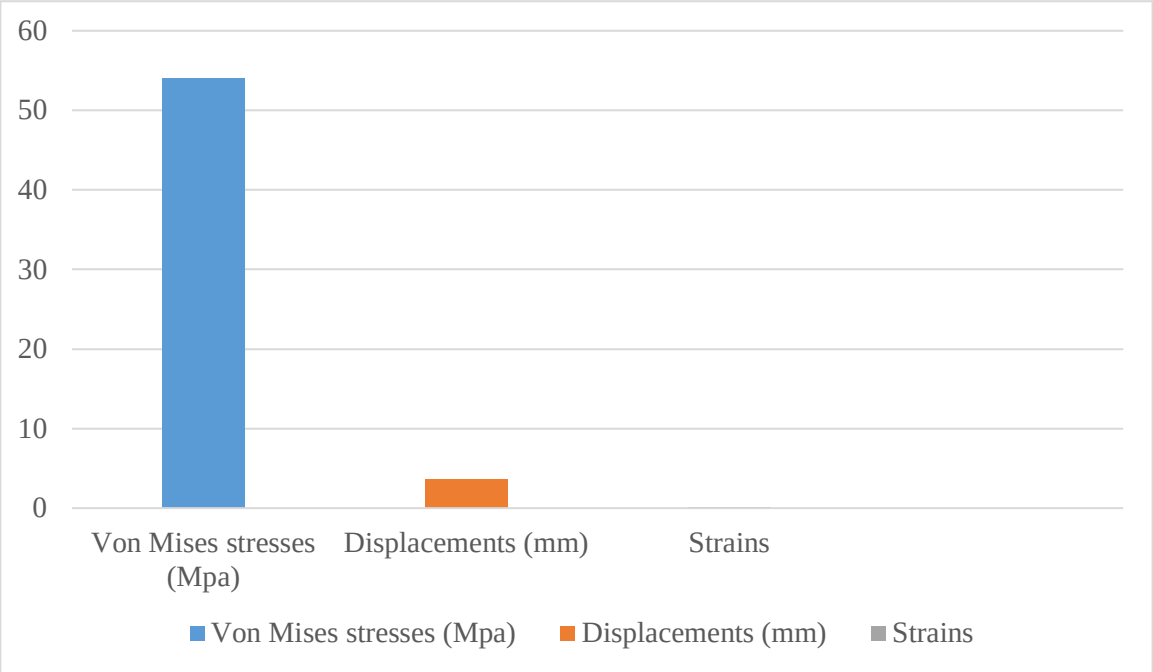

Fig. 15. Vertical drop test from 3m height, simulation results

It was observed that during the first drop test where the drone falls flat from 3m height. Very large stress forces of 54MPa appeared between the connections of the wings and the frame pieces. Also, the maximum displacements 3.6mm, observed at the center of the frame, higher strains forces of 0.014, appeared also between the wings and the main body.

- **Drop test 2**

Initial settings: Velocity at impact = 26 m/sec^2, Gravity 9.81 m/sec^2, Target is normal to front side of quadcopter, Rigid tarter, Contact damping = 1.

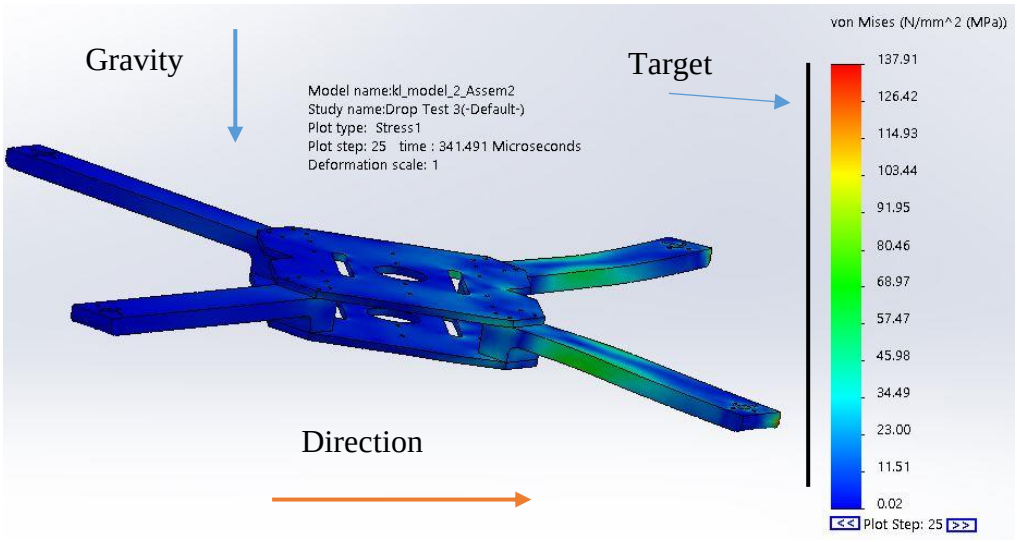

Fig. 16. Impact test, Von Mises stress plot

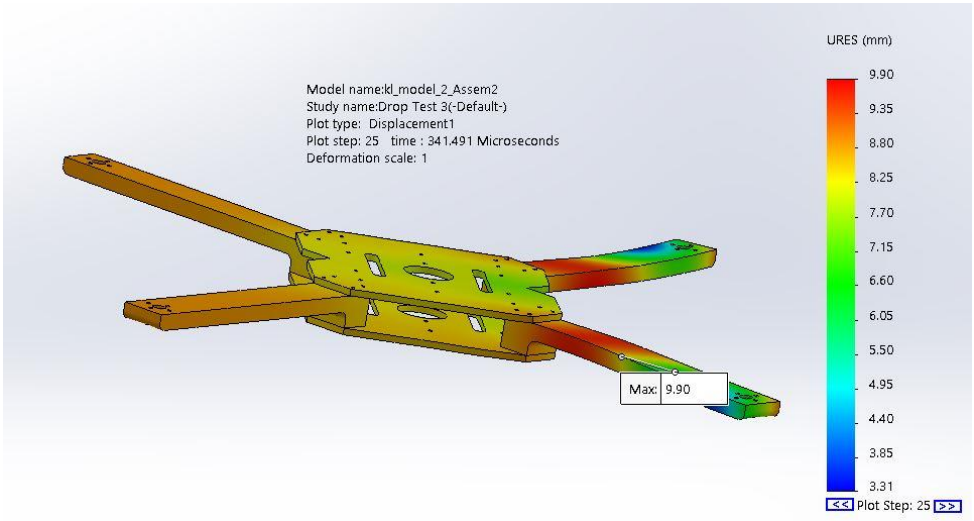

Fig. 17. Impact test, displacement plot

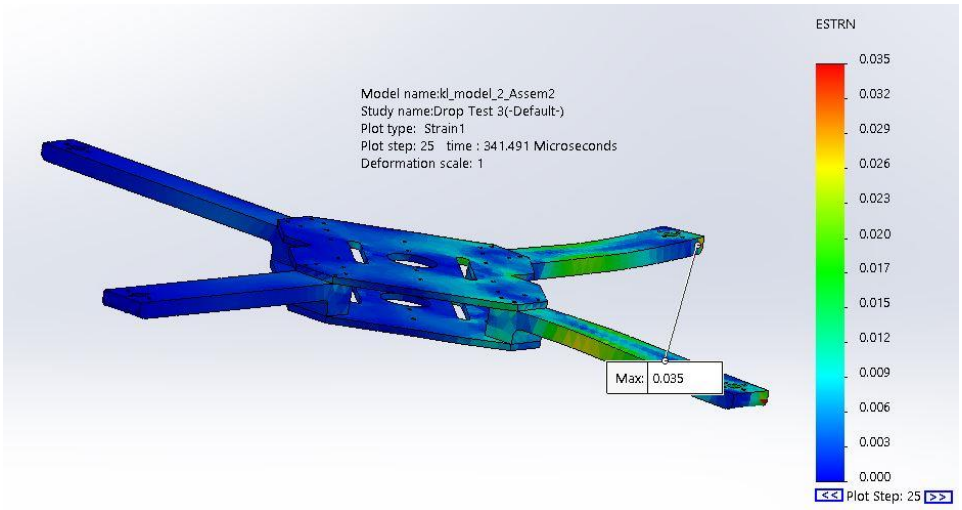

Fig. 18. Impact test, strain's plot

It was observed that during the second drop test where the drone crashes into a rigid virtual wall. Very large stress forces (137.9MPa), appeared on the side which comes first in contact with the wall. Also, the maximum displacements (9.9mm), and strain forces (0.035), observed at the same points.

3.1.3. Results of finite element analysis

The results of each test conducted for the frame of the quadcopter can be seen on Table 7.

Table 7. FEA Simulation Results

Quadcopter State	Max Stresses - Von Mises (MPa)	Displacements (mm)	Strain
Take-off	3.02	2.68	0.001
Hovering	2.78	2.47	0.001
Moving forward (Pitch)	2.77	2.62	0.001
Drop test 1	54.23	3.63	0.014
Drop test 2	137.92	9.90	0.035

From Table 7, was observed that during all three flight states, the maximum stresses acting on the quadcopter frame are much lower than the maximum tensile strength of the selected material. Also, very small displacements were observed at the area which the motors of the quadcopter are located.

During take-off state were observed the highest values for stress and displacements, which is normal since the lift forces acting on the quadcopter must be greater than the weight of the drone.

Moreover, the results of the drop test's showing very larger stresses and displacement which are above the yield limit. In these cases, the frame would fail to maintain its rigidity and brake. For these reasons, its necessary to design supports on the areas where the maximum stresses are observed and to include guarding covers which can protect the electronic components of the system.

Table 8. Comparison of both designed frames under 3kg of load

Quadcopter State	Max Stresses - Von Mises (MPa)	Displacements (mm)	Strain
Model 1 (Compact design)	22.8	11.8	00.78
Model 2 (Improved frame)	3.02	2.68	0.001

Table 8 presents the results of the finite element analysis of the improved design and the previous compact design made for aerial thermography under 3kg of total load. The improved design presents significantly lower number of maximum stresses, displacements, and strain forces in comparison with the previous compact design.

3.2. Quadcopter electronics

The second step after the design of the customized drone frame is the selection of the electronic components which are necessary in order to make the designed drone operational.

3.2.1. Actuators

In this case the most commonly actuator used for small to medium drone designs are brushless DC motors due to their simple mechanical design and comparatively simple control.

Normally a brushless direct current motor or BLDC consist of two parts, a rotor, and a stator as shown in Fig. 19. There are two types of BLDC motors, in-runner motors where the stator is equipped with armature windings while the rotor consists of a permanent magnet, and out-runner motors where the stator acts as permanent magnet, and the rotor is equipped with armature windings. In case of an in-runner BLDC motor when current is applied on the coils of the stator, a magnetic field is generated according to the current's direction. This current tends to attract the permanent magnet on the rotor. If then each coil is activated in sequence, the rotor keeps rotating due to the present attraction forces. The rotation of the rotor will produce the necessary motor torque Tm, which is required to spin the propellers attached to the motors. The opposite applies for the out-runner BLDC motors. Brushless motors can be single, two, or three phases accordingly and rotors can have from two to eight pairs of permanent magnets.

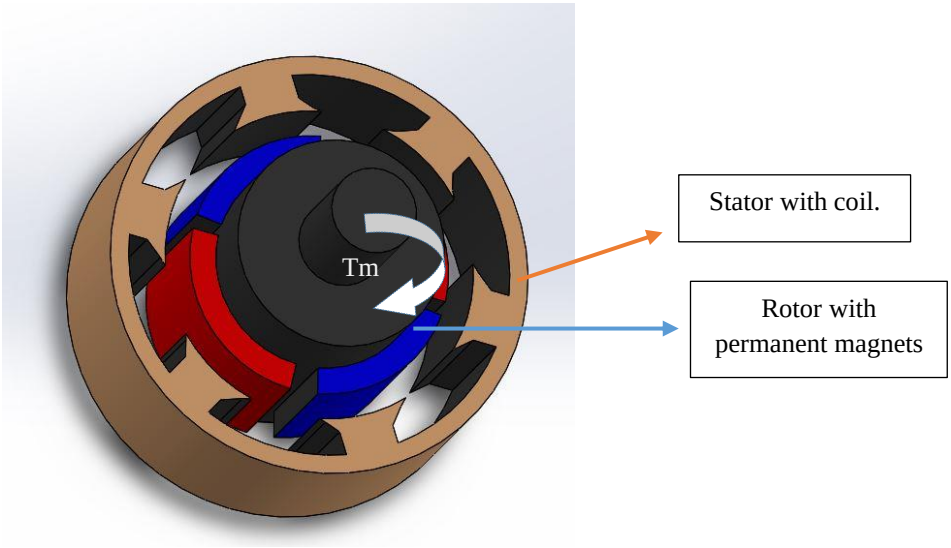

Fig. 19. Motor torque Tm produced by BLDC in-runner motor SolidWorks sketch

The commercially available BLDC motors for drone applications are three phase motors and normally are described by two numbers, for example RS 2306 - 2750KV, the first four-digit number indicates the diameter of the stator (23mm) and the high of the rotor (06mm), the second four-digit number indicates the maximum rpm of the motor when 1V is applied under no load to the motors. Although the maximum rpm which a motor can achieve for the drone system depends on the power source of the system. For this project, a 3S 2200 mAh battery and four. 2213 – 920KV brushless motors are selected, the maximum RPM produced by the selected motors can be calculated as [23]:

RPMmax = Motor KV x Battery = 920 x 11.1 (3S Battery = 3.7V per cell) = 10.212 RPM

In order to control a BLDC motor, generated digital signals of 50Hz in frequency are required. This is achieved by using pulse width modulation or PWM method of signal controlling. These signals work as ON or high 5V and OFF or low 0V, pulses which their length can be controlled. By controlling the width of the digital signal, the energy provided to the load is also changing. An example of PWM signal controlling servo motors and brushless motors can be seen in Fig. 20.

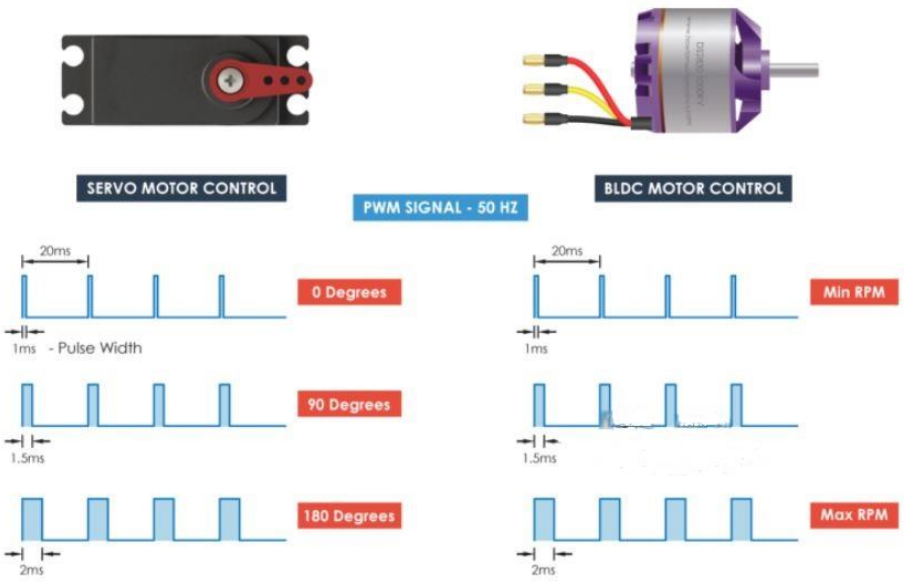

Fig. 20. Servo motor and BLDC motor speed control by PWM as seen on an oscilloscope [23]

In case of servo motors, change on the width of the digital signal will cause the position change of the motor end while in BLDC motors width change is translate as faster or slower revolution of the motor.

3.2.2. Propellers

Depending on the design of the frame and the selection of the motors the necessary propellers can be selected. The propellers are used to transform the rotational motion to upward lift. Blade element theory is used in order to predict the overall performance of the selected propellers. According to this method the blade of the propeller is divided into smaller parts where calculation of the air forces acting on the propeller blade is possible. Fig. 21 presents the division of the propeller into smaller elements each with different radius. The different lift and drag forces on each section can then be calculated by standard airfoil properties for a blade of pitch angle (θ) [24].

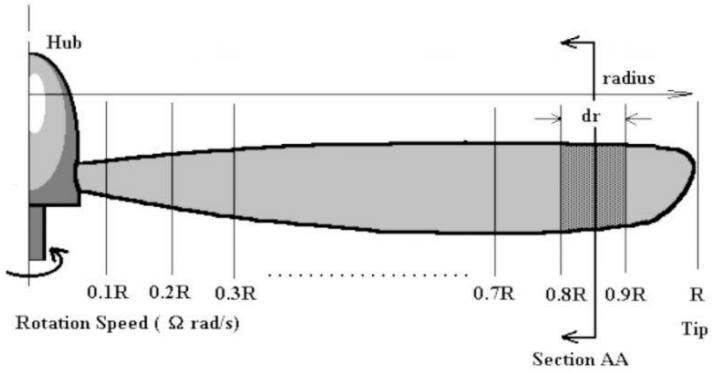

Fig. 21. Division of drone propeller into smaller elements [24]

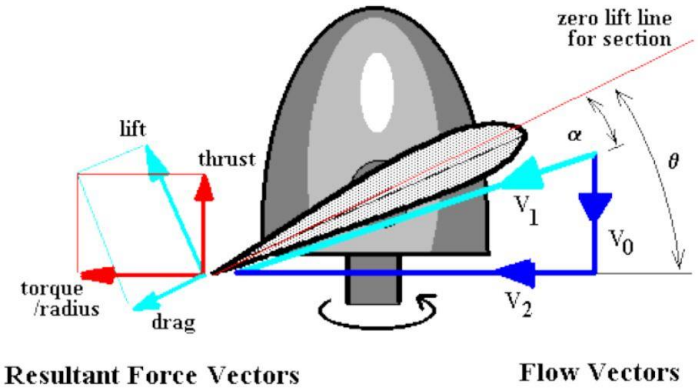

Fig. 22. Forces acting on the blade, V0 is the axial flow & V2 is the angular flow acting on each element[24]

Is assumed as (φ) the angle difference of thrust and lift angles,

$$\varphi = \theta - \alpha$$

For a particular segment of the blade, the elemental thrust, and torque equations are,

$$\Delta T = \Delta L \cos(\varphi) - \Delta D sin(\varphi)$$

$$\frac{\Delta Q}{r} = \Delta D cos(\varphi) + DL sin(\varphi)$$

By applying the airfoil coefficients for a given angle (α) the below equations derive,

$$\Delta L = CL \frac{1}{2} pV1^2 c.dr$$

$$\Delta D = CD \frac{1}{2} pV1^2 c.dr$$

CL and CD represents the lift and drag coefficients. As p, is defined the density of the air and c.dr is the lift producing area or the blade segment. For given number of propeller blades (B), the complete elemental equations for thrust and torque are,

$$\Delta T = \frac{1}{2} pV1^2 c\big(CLcos(\varphi) - CDsin(\varphi)\big)B.dr$$

$$\Delta Q = \frac{1}{2} pV1^2 c\big(CDcos(\varphi) + CLsin(\varphi)\big)B.dr$$

The efficiency of a propeller is derived by the equation,

$$\eta = \frac{DTV}{DQ2\pi n}$$

And is described as the ratio of the useful power divided by the absorbed power.

The shape of the blade makes difficult the implementation of single expressions describing the thrust, torque, and efficiency of a propeller thus the results acquired for a single section of the propeller describe the rest section of the propeller. Fig.23 shows the shape of blades, the coefficient values for thrust and torque, and the total efficiency between two propellers (1045 blade left, and 5045 right). The calculations made with the free of charge application provided at [24].

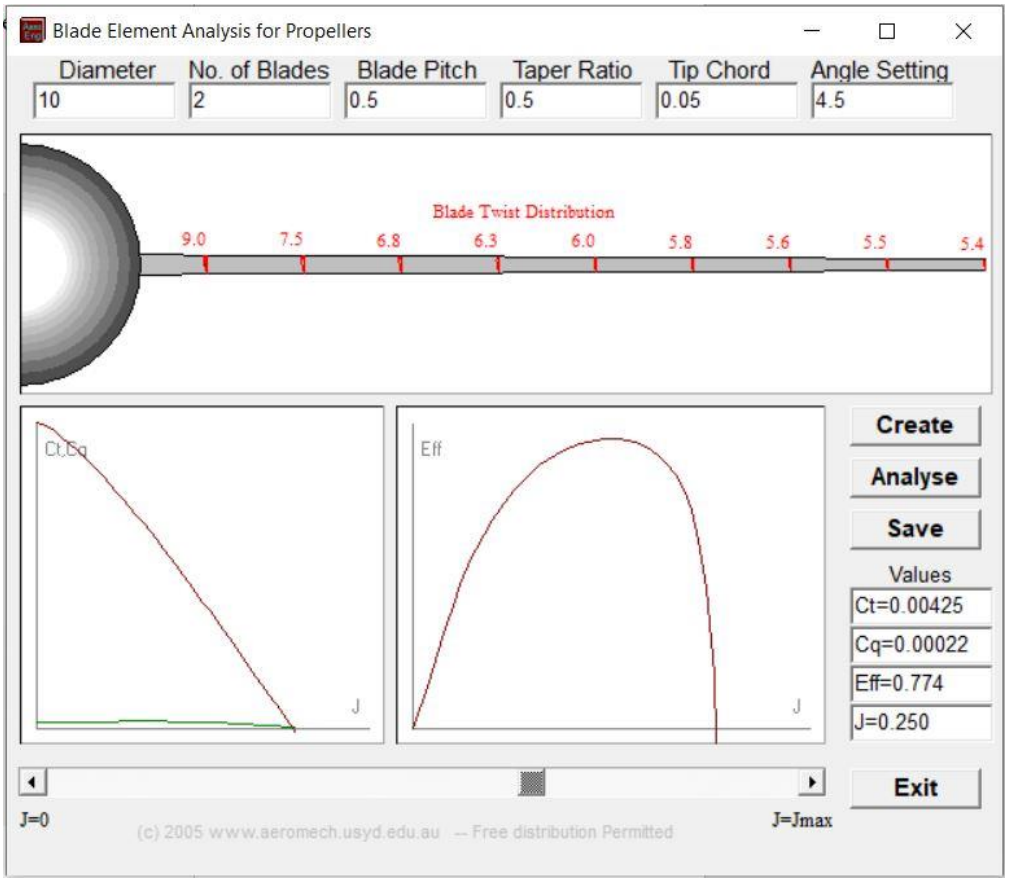

a

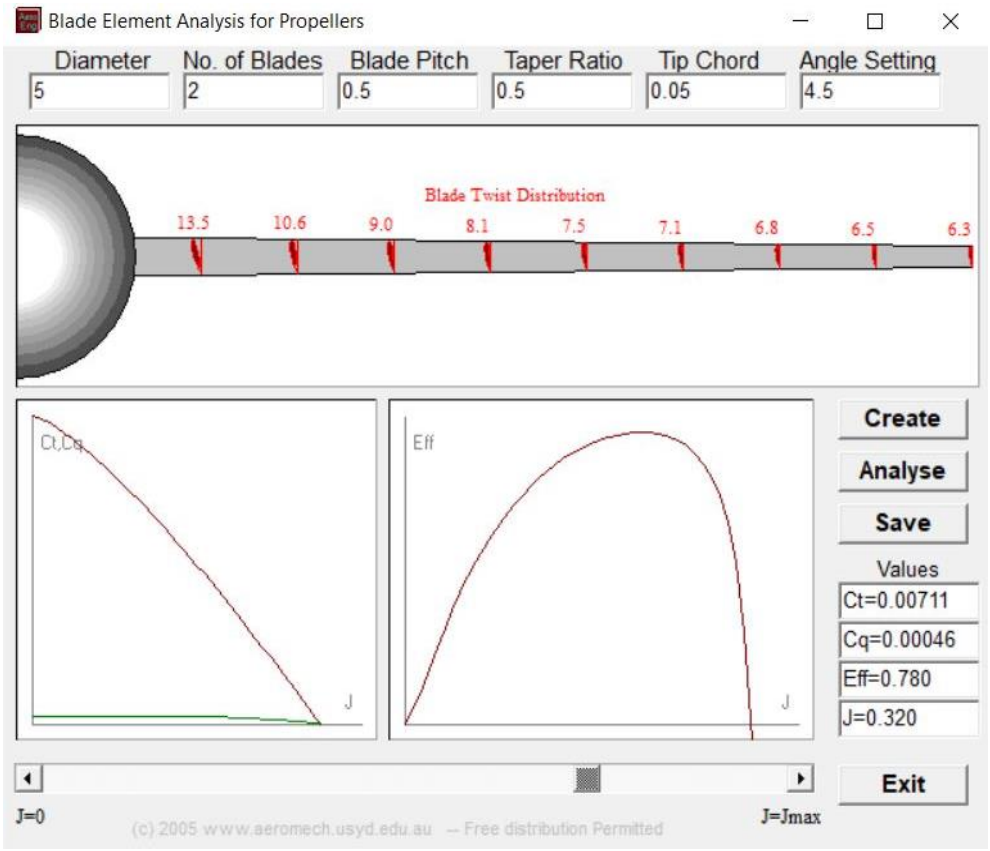

b

Fig. 23. Blade element analysis results for 1045 (a) and (b) 5045 size propeller blades

Fig. 23 shows that 1045 blades reach maximum efficiency η=0.774 when 0.250J is consumed while 5045 blades require 0.320J to reach maximum efficiency of η=0.780. There is not significant difference on the results although it is known that bigger size propeller produces more thrust which is required for lifting heavier payloads [25].

3.2.3. Electronic speed controller (ESC)

Drones and small type UAV's use electronic speed controllers in order to adjust the motors speed. An ESC transforms DC voltage supplied from batteries into AC current suitable for motor speed control. Other ESC's functions are to control the rotation of the motor, to slowly start the motor rotation in order to avoid sadden speed changes causing unpredicted control by user (soft start), and also indicate low voltage alarms to inform the user when power is running down (motor rotation reduces gradually). Different manufactures (Opto, X-rotor, BL-Heli, Simonk), provide different type of ESC'S depending on the maximum amperage which an ESC can operate (from 6A to 30A or more), also calibration of ESC's is required in order to set the maximum and minimum limits of an ESC according to the received control signal (transmitter communication signals). Calibration instructions, software upgrades, and other ESC's functions are provided by the manufacturers of each brand. An ESC connection with a motor is shown in Fig. 24.

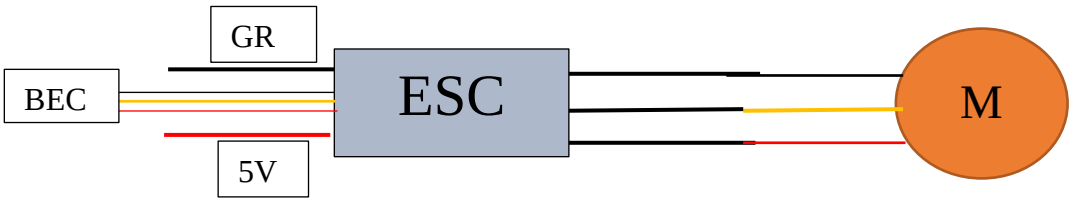

Fig. 24. ESC connection with motor

In order to determine the speed of a motor, the ESC uses proportional feedback signal derived by the equation [23]:

$$Vm = K (\omega_D - \omega)$$

Where ω is the angular speed of the motor, ω_D is the desired angular speed and K is the motors constant.

An ECS has three cables for connection with a three-phase motor on one side and two cables for powering the ESC (red 5V and black ground), on the other side. Some ESC's have another set of cables which are used for powering of other devises directly from the ESC unit without the use of external connection with the battery. This function is called battery eliminator circuit or BEC.

3.2.4. Flight controller (FLC)

UAVs require systems which are able to process data, follow instructions and execute commands in order to initiate, plan, or maintain flight. For this role specialized microcontrollers have been developed. Such microcontrollers called flight controllers or FLC's. A flight controller is responsible for receiving data by internal sensors such as gyroscopes (rotational motion), accelerometers (lateral movement), barometers (altitude), and GPS (location) sensors, processing them and giving commands to the ESC's in order to adjust the rotation of the motors accordingly, by doing so stable flight conditions can be achieved.

Drone stabilization during flight is a very important task which is influenced by many parameters. Sadden chances in drone position due to external forces such as wind gusts, make difficult the control of the drone. Most common method used for drone stabilization is through proportional interval derivative (PID) controllers. These controllers can process measurements taken by onboard sensors and fed back signals to the flight controller CPU where the necessary calculations are made in order to adjust the power given to the motors. By doing so the drone can adjust its position in order to maintain stable position.

Flight controllers are connected with ground controllers or so-called transmitters via electromagnetic signals. The user is able to send control commands to the flight controller in order to manually control the position and orientation of the drone. The transmitted signals are received through a paired receiver connected on the flight controller. FLC's can also be connected to camera modules for live broadcasting of sound and image.

Along with the hardware part, flight controllers come with specialized software which enables the user to calibrate the measuring units of the system. Also, the user is able to create different flying modes and store them in the memory of the system. These modes then are available for selection through designated buttons on the transmitter.

For this project, an Arduino Mega microcontroller is used as the main flight controller of the system. A PID controller made by [26] is the main control algorithm needed for this project and is loaded into the Arduinos memory. The block diagram used for implementing the PID controller can be explained by the Fig. 25.

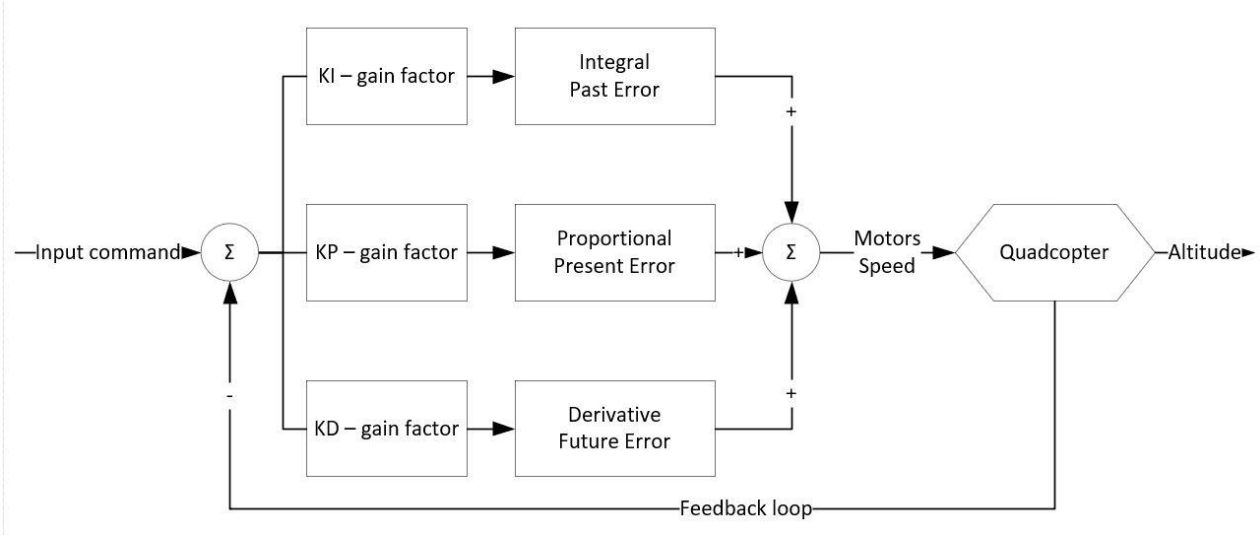

Fig. 25. Block diagram of PID controller designed for quadcopters, drawing made in Visio

The controller of the Fig.32 can be expressed by the equation:

$$u(t) = kpe(t) + ki\int_0^t e(t)dt + kd\frac{d}{dt}e(t)$$

Where kp, ki, and kd are gain factors for the present, past, and future errors calculated by the PID controller. For this system, the configuration of the controller can be written as:

- Proportional = error value x kp gain value **OR**

Proportional output = (gyro value – receiver value) x kp

- Integral = sum of the errors x ki gain value **OR**

Integral output= Integral output + ((gyro value – receiver value) x ki

- Derivative = difference between current and previous errors x kd gain value **OR**

Derivative output = (gyro value – receiver value) – (past gyro value – past receiver value) x kd

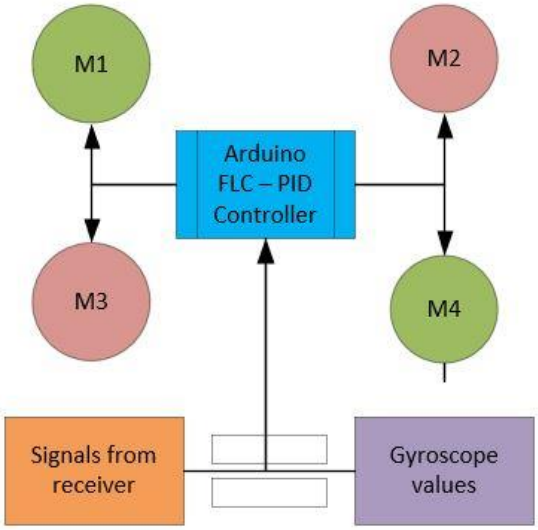

Fig. 26. Arduino flight controller, drawing made in Visio

The main purpose of the PID controller is to maintain the drone in a stable state when there are no command signals send from the user to the drone via the transmitter – receiver communication as shown in Fig.26. In other words, the controller reads the angular rate values from the gyroscope and calculates the correction values needed in order to retain the drone's current stable state. For this system, an MPU-6050 inertial measurement unit is used. This sensor is equipped with a 3-axis accelerometer, a 3-axis gyroscope and a digital motion processor which can communicate with the Arduino board through I^2C communication protocol.

3.2.5. Rest of electronics

To complete the quadcopter system a few more parts are necessary. As power source the drone uses a 3S Lipo rechargeable battery which can provide maximum 11.1 V (3.7V per cell). For video and audio broadcast a Boscam FT952 video transmitter with its antenna and AV connection cable (to connect with thermal or another camera) is selected. Finally, a Flysky fs i6x 2.4 Hz 10 channel transmitter and a Flysky fs-ia10b 10 channel receiver are the selected components in order to complete the system.

Table 9. Mass of system components

Part	Name	Quantity	Total mass (grams)
1	BLDC motor &props	4	240
2	Electronic speed controller	4	112
3	Arduino FLC	1	27.2
4	IMU MPU-6050	1	5
5	Battery	1	355
6	Payload 1 (Thermal camera)	1	65
7	Drone frame	1	380
8	Power distribution board	1	7.5
9	Receiver	1	9.5
10	Video transmitter	1	15
11	Payload 2 (Robotic arm)	1	343
12	Rest of hardware	X	150
Total mass			1709.2

From Table 9, the total load of the proposed system is calculated at 1.7 kg. For these calculations, the mass of the drone frame, drone electronics as well as of payload 1 and 2 is considered.

3.3. Design of aerial manipulator

Additionally to the existing payload selected on [13] for aerial thermography, a custom made manipulator arm is designed in order to provide enhanced possibilities to the existing system. The robotic arm can expand the available options of the system by introducing multiple attachments which can then be used in order to perform various contact and contactless non-destructive maintenance techniques. Robotic arms have been designed and used in many cases and for different applications as was presented in [6,7,8,9], deployment of such systems is an advantage to the end user since it minimizes the time of interventions in comparison to the standard methods which require extensive

preparations in order to perform the required activities. Moreover, aerial manipulators can be used in environments which are hazardous without risking the health and safety of the system operator since the control and navigation of such system can be performed autonomously or semi-autonomously from distant safe zones.

For this system, a compact light weight manipulator with total 4 DOF is designed in order to provide the possibility of attaching an NDT measuring unit and its probe for contact type testing in the existing system. By doing so a versatile system equipped with multiple NDT methods can be realized. In this case multiple testing methods can be realized simultaneously without the need of extra preparations.

In addition, the system can be further customized by attaching various grippers as end effectors to provide grasping capabilities for carrying and transporting equipment or other materials.

3.3.1. Design constrains

Since the robotic arm is attached to the main frame of the quadcopter, constrains such as the weight of the arm and the inertia forces produced during arm actuations must be considered. The total weight of the payloads must be lower than the maximum payload which the drone can carry. Also, lower inertial forces can be realized by placing the arm components closer to the center of mass of the structure. By doing so, the influence of the arm motion over the drone's stability can be minimized [27]. These constrains can be defined by the equation:

$$Drone_{Weight} + Payload\ 1 + Payload\ 2 + Extra\ payload \leq \eta\ \times Available\ Payload$$

The drone weight is equal to the total weight of all selected components including the frame, landing gear, and electronic components. Payload 1 is the load of the thermal camera. Payload 2 includes all hardware parts required for the construction of the robotic manipulator. Available payload is the maximum load which the drone can carry multiplied by a safety factor η=0,75.
From the above formula derives:

$$1.7kg + \ Extra\ payload \leq 0.75 \times 3.4kg =>$$

$$Extra\ payload \leq 0.85\ kg$$

The calculations above shown that there are at least 0.85 kg available for extra payloads.

3.3.2. Materials used

The robotic arm designed for this application consists of four servo motors and six custom-made parts designed in SolidWorks. Custom servo holders are made in order to attach the servo motors to the frame of the robotic arm. The parts can be 3d printed on the same way as the quadcopter frame parts. All parts of the robotic frame can easily be customized and re-designed according to the requirements of the user.

As main actuators, two Miuzei DS3218 high torque servo motors and two Lobot LX-224HV are used to produce the required force to realize the arm motion. Figure 27 shows the selected servo motors and their characteristics are described on Table 10.

Fig. 27. Servo motors a) Miuzei DS3218 and b) Lobot LX-224HV [14]

Table 10. Servo motors specifications [14]

Specifications	Miuzei DS3218	Lobot LX-224HV
Operating Voltage	4.8 to 6.8 V	6 to 12V
Current draw at idle position	4mA at 5V / 5mA at 6V	NA
Stall torque	18kg at 5V / 21.5 kg at 6.8V	20kg at 7.4V
Gear type	Metal gears	Metal gears
Control system	PWM	PWM
Mass	60 grams	63 grams
Shaft output	Single	Single - double mounting
Operating temp	-15 to 70 °C	NA
Cost (Eur)	18 Eur	15 Eur

The basic difference between these two selected servo motors is the double mounting pads on Lobot servos which are designed for robotic applications. Otherwise, both servos present similar characteristics.

3.3.3. Robotic arm overview and simulation

The designed robotic arm can be seen on Fig.28. Looking from the top right corner the first servo motor is attached to the frame of the quadcopter and is responsible for the yaw motion of the first join. Next is another servo motor attached to the first servo on one side which is responsible for the pitch motion of the first limp. At the end of the first limp is another servo motor also connected with the second limp and can produce pitch motion too. Lastly an attachment point for various equipment is connected on the shaft of the fourth servo motor.

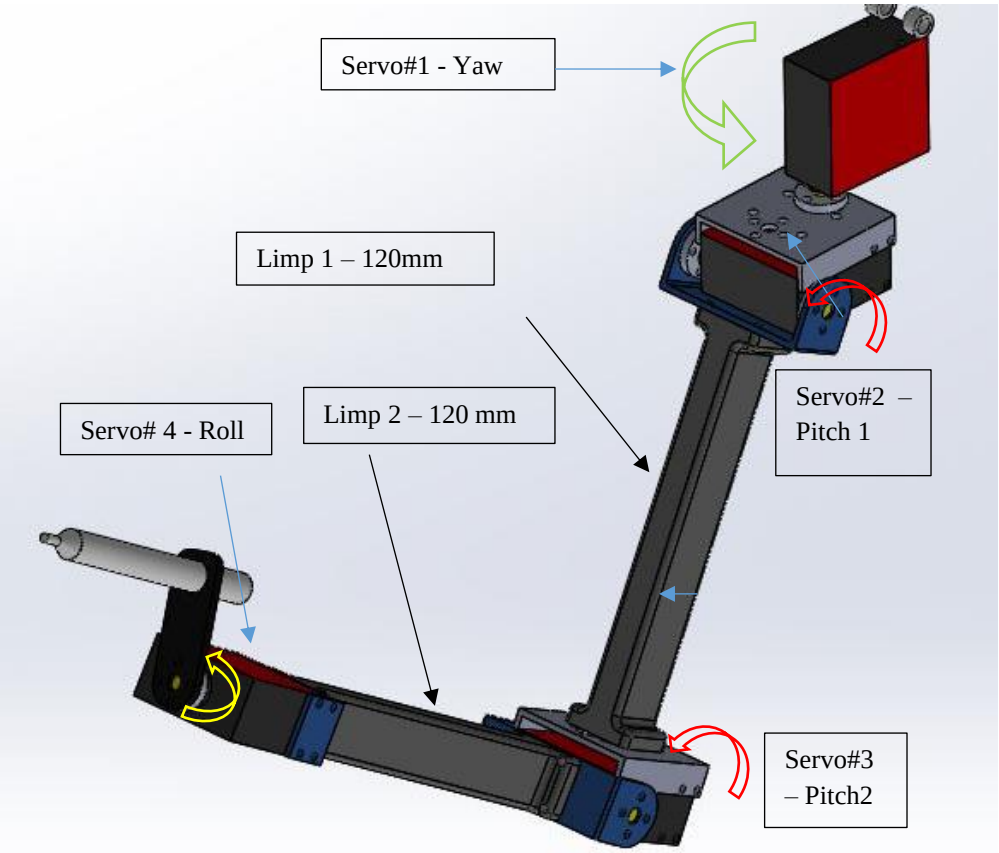

Fig. 28. 4 DOF Robotic arm assembly made with SolidWorks

The size of the two limps determines the maximum reach that the end effector can achieve. Although, constrains such as the quadcopter landing gear and propellers limit the range of the first joint motion (yaw) and the third servo motor (pitch No2).

To simulate the motion of the robotic arm, the assembly model was exported into Matlab Simulink environment where an automatic 3d model was created based on the design made in SolidWorks. Simulink environment is an add-on software provided by Matlab which allows the user to create interactive graphical models of dynamical systems. By doing so the model can be simulated and analyzed through the provided graphical user interface. Every model consists of blocks which are available in Simulink libraries, the blocks are connected with lines in order to assemble a block diagram of the designed system.

To export any kind of model into Simulink environment, the Simscape Multibody Link add-on is required. This add-on is installed into Solidworks software and enables Solidworks to create the necessary file extensions (.xml), which can then be imported into the Simulink environment.

The robotic assembly file was exported through SimMechanics Link available in SolidWorks - Tools directory. Then on Matlab by using the ‘smimport(‘file_name’) command, the assembly model is imported.

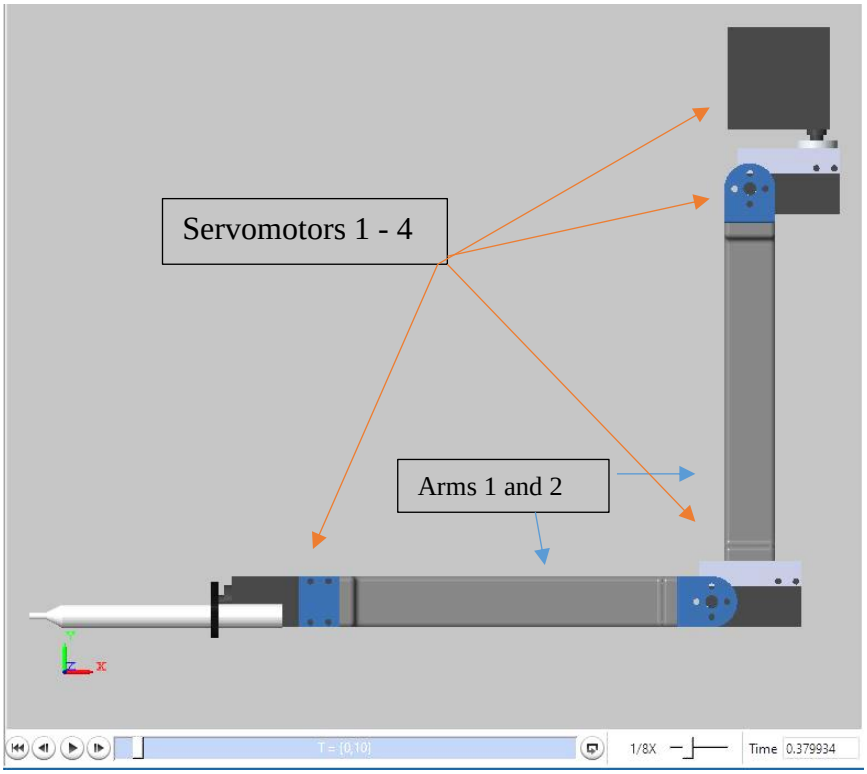

Fig. 29. Robotic arm model on Matlab Simulink simulation environment

After importing the assembly model to Matlab Simulink environment as shown in Fig, 29, the software creates an automatic block diagram of the existing assembly based on the constrains made in Solidworks. The block diagram includes all the parts used for the assembly linked together as can be seen on Fig. 30.

Custom sliders have been included in order to set limits to the motion of the joints. Also, by adjusting the values of the sliders the position of the manipulator changes accordingly.

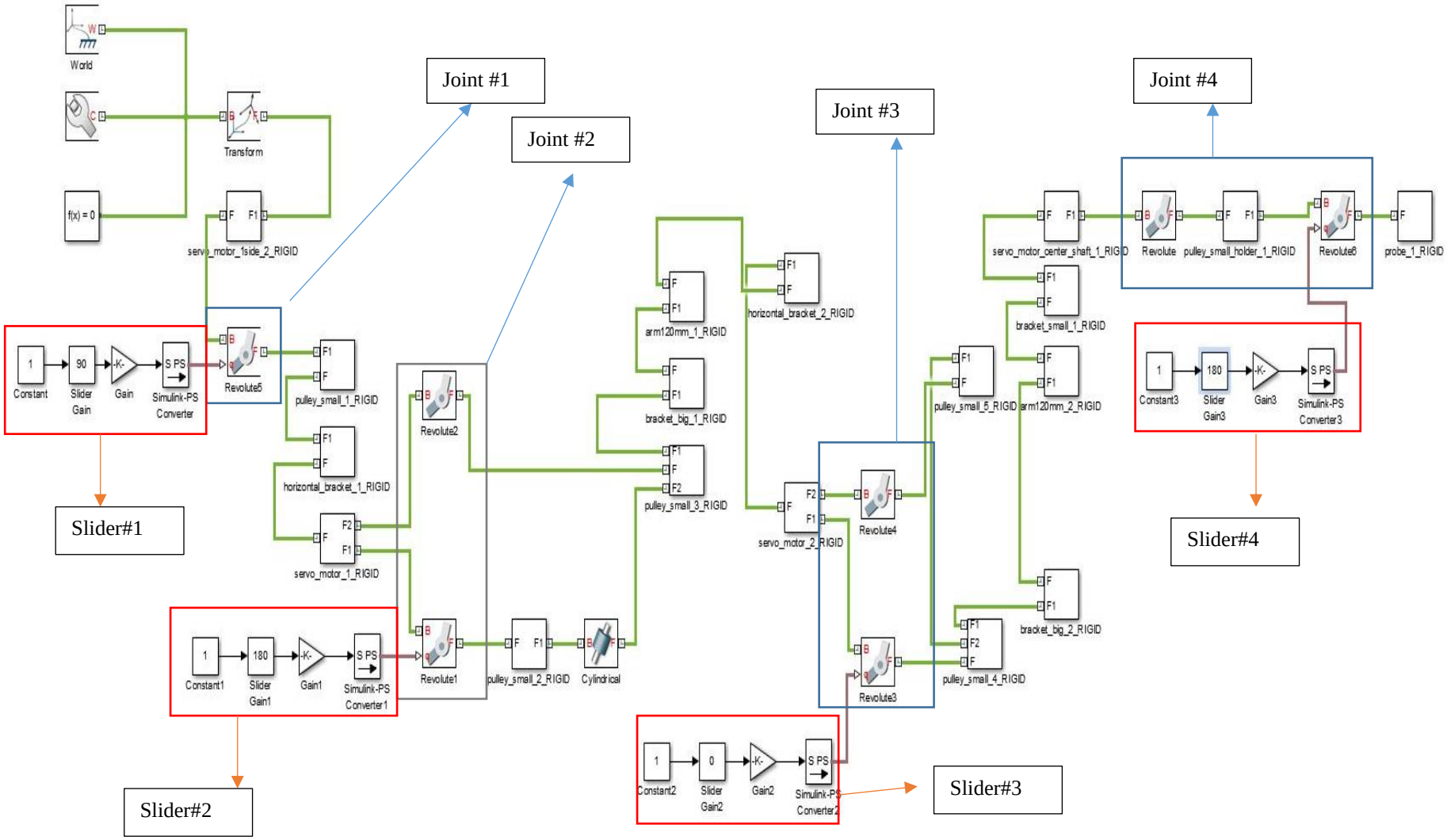

Fig. 30. Block diagram of robotic manipulator made with Matlab Simulink environment

.

3.3.4. Wiring diagram of improved system

The wiring diagram of the proposed improved system is presented on Fig.31. For this system, each brushless motor is connected to an individual electronic speed controller while the signal wires for controlling the motors are connected with the Arduino digital ports D6, D7, D8, and D9. The Arduino flight controller gets signal commands from the ground transmitter through the receiver. Four wires one for each brushless motor are connecting receiver channels 1 to 4 with Arduino digital pins D10, D11, D12, and D13. The inertial measurement unit is connected to the Arduino's ports SDA and SCL which are designated for I^2 C communication. This protocol is used for communication of a master devise (Arduino Mega), and multiple slave devises, in this case the Inertia Measurement Unit (IMU). Data from the IMU sensor are transmitted through the serial data port (SDA), while SCL is the serial clock connection.

For the control of the robotic arm, same connection method is applied. Digital ports D2, D3, D4, D5 are used for controlling servo motors 1 – 4 while D14, D15, D16, D17 ports are connected directly with the receiver module. A LED is connected with digital pin D38 and will lit when the battery voltage drops. The battery voltage is monitored through the analog port A0. Lastly a distribution board connected with the battery provides all the necessary power and ground ports to each component of the system.

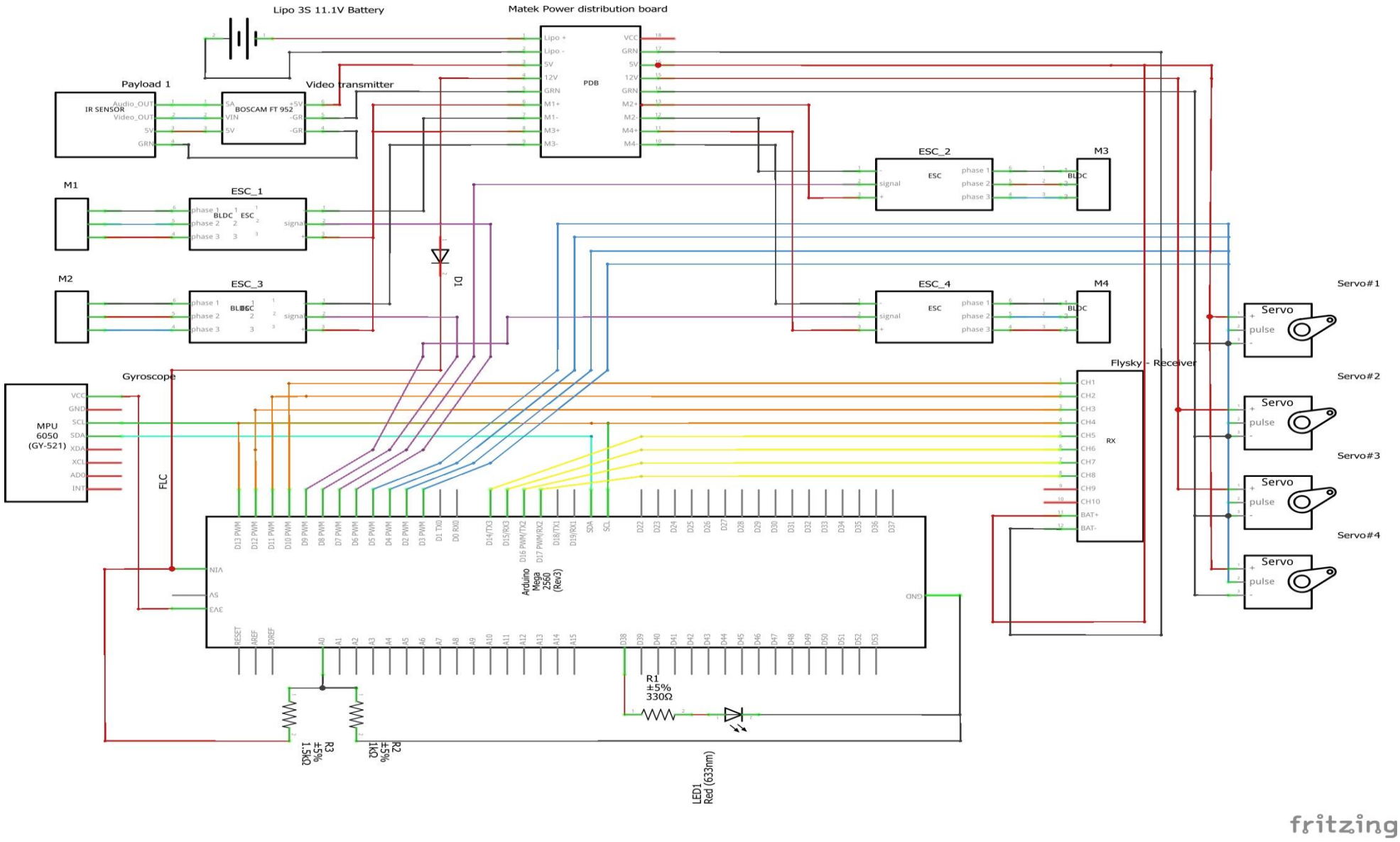

Fig. 31. Wiring diagram of improved system, made with Fritzing

3.4. Assembly of proposed system

The assembly of the proposed system consists of two main sub-assemblies. The first sub-assembly is the assembly made for the customized quadrotor drone which contains all the electronic components the frame parts and the first payload (thermal camera). The second sub-assembly is the robotic manipulator which adds extra 4 DOF on the existing system. As result a 10 DOF adaptable system is created. All the components selected for this system are parts which can easily be interchanged with other similar parts depending on the requirement of the user. The drone frame parts, and robotic arm limps can be printed by using any 3D printer which can load .stl files. This is an advantage in comparison with other materials since in case of damage or crash the frame parts can easily be replaced within a few hours minimizing the cost of procuring new parts. The complete assembly of the proposed system can be seen in Fig. 32.

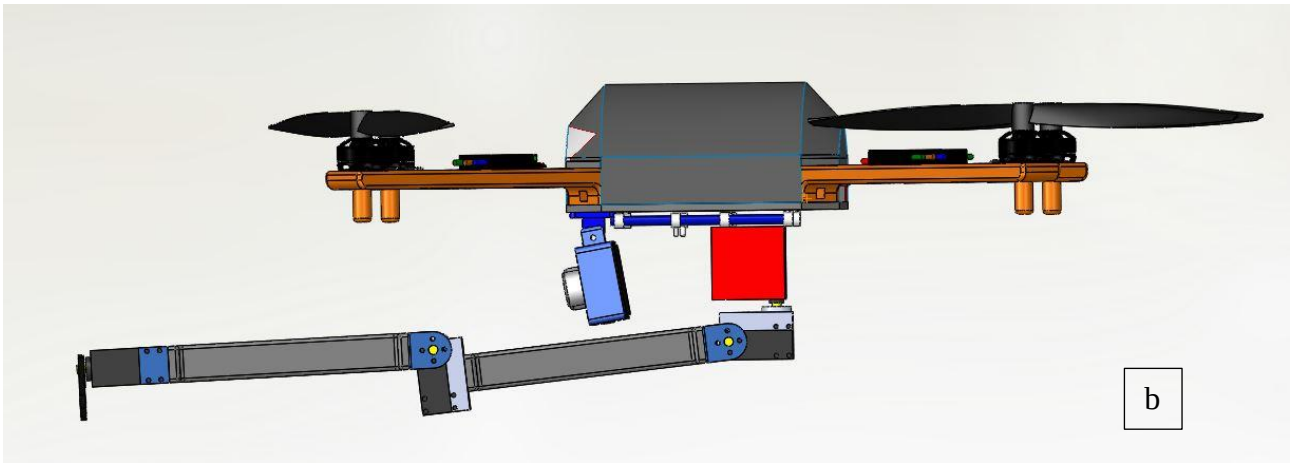

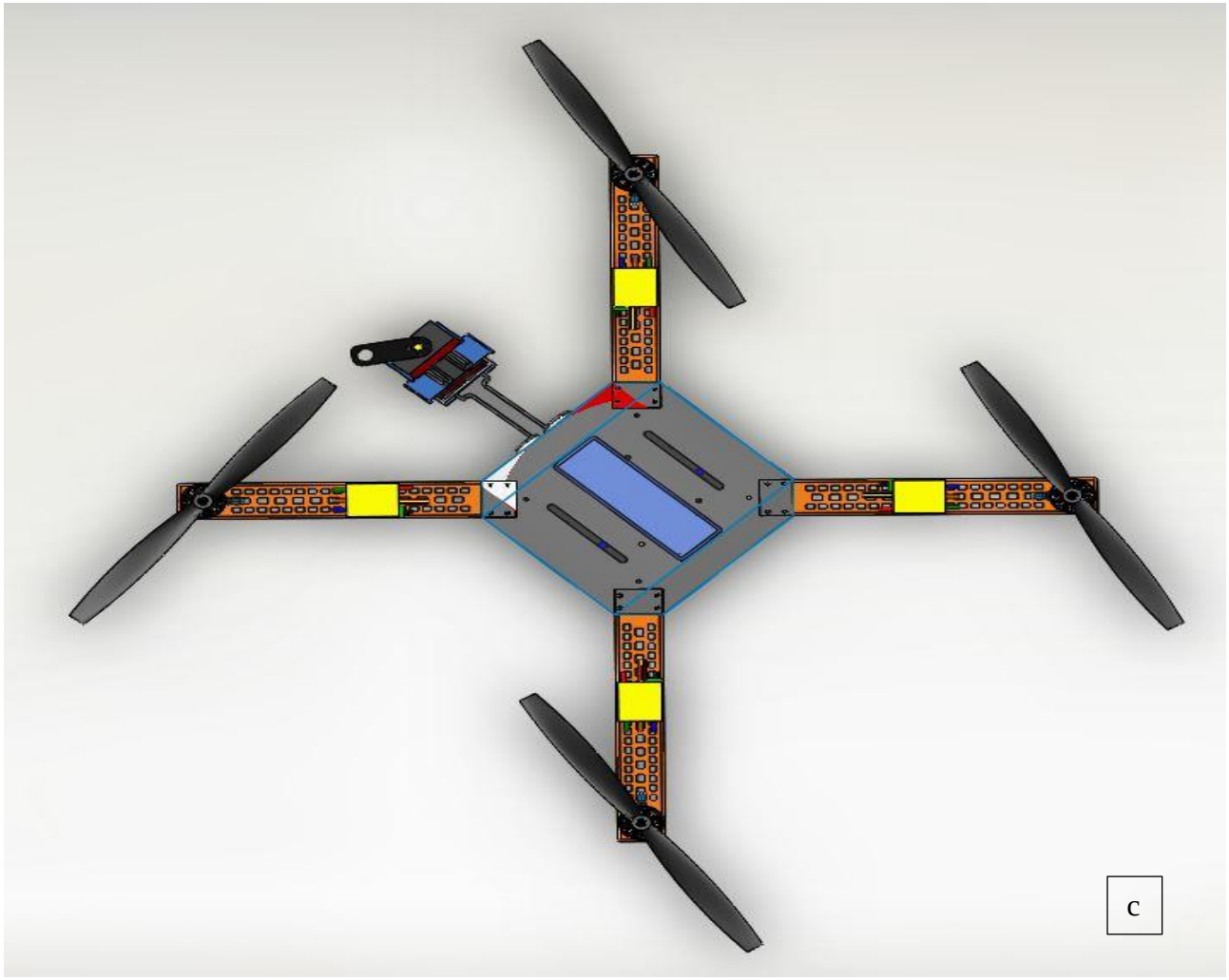

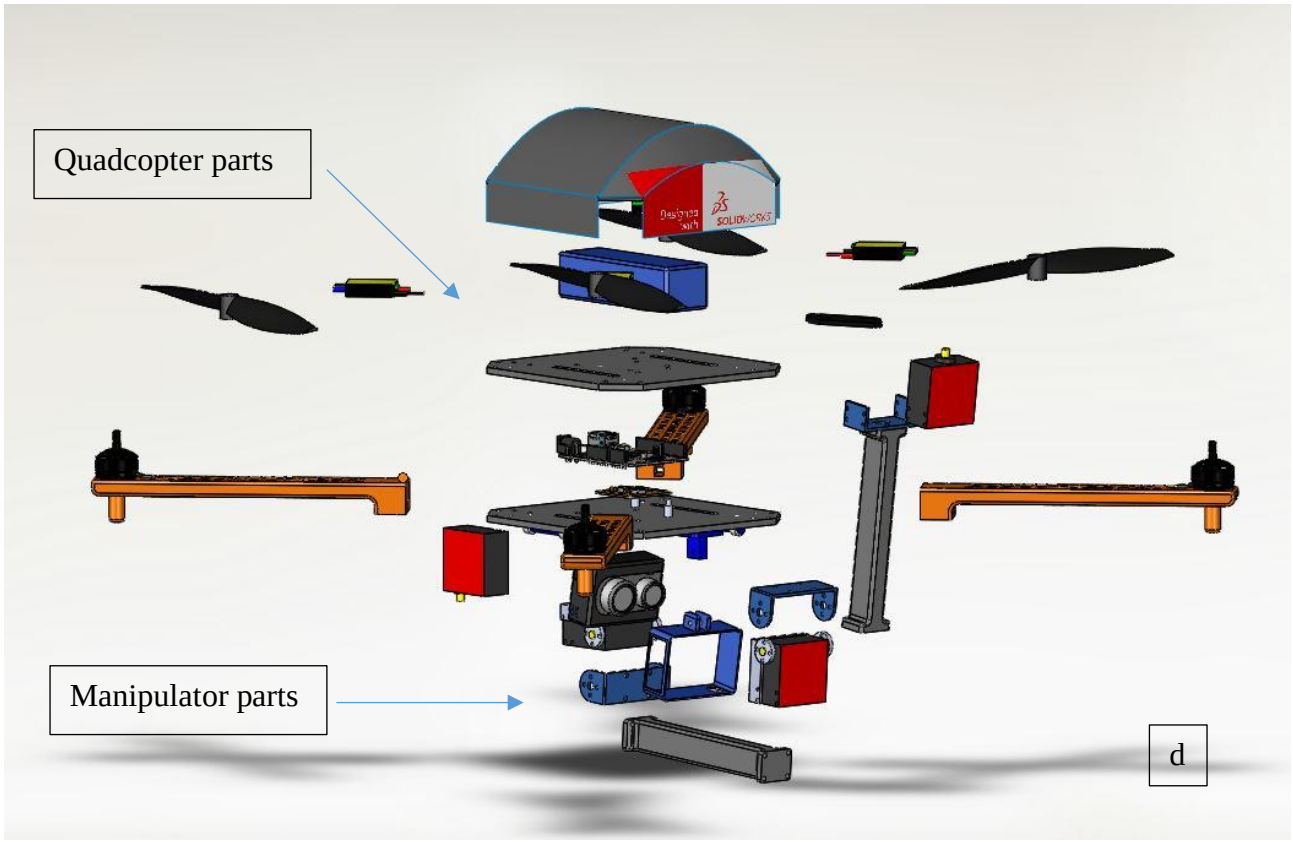

Fig. 32. Views of the assembly made with SolidWorks a) Isometric b) Top c) Side view d) Exploded view

The landing equipment is not shown on the Fig.32. above although attachment points have been created under the bottom plate in between the two payloads.

3.5. Total flight time calculation

Given the total load of the designed system at 2.5kg and battery capacity of 5200mAh estimation of the total flight time can be done by [28]:

$$Total\ Flight\ Time = \frac{Battery\ Capacity\ \times\ Discharge}{Average\ Ampere\ Drawn}$$

The Average ampere drawn by the selected motors can be calculated by:

$$Average\ Ampere\ Drawn\ =\ Total\ payload\ of system\ \times \frac{P}{V}$$

Where P is the required power for lifting weigh of 1kg, for brushless motors P=100W/KG, and V is the total voltage of the selected battery.

$$Average\ Ampere\ Drawn\ =\ 2.5kg\ \times \frac{100W}{11.1} = 22.5\ A$$

Given that the Total flight time can be calculated as:

$$Total\ Flight\ Time = \frac{5200mAh\ \times\ 85\%}{22.5\ A} = 11.77\ min$$

The total flight time of the proposed system is calculated at 11.77 min. For these calculations it was consider that the total load which the drone is carrying is maximum (2.5kg).
Although, considering the current applied load (drone parts, and payload 1,2) the maximum load is calculated at 1.7kg which increases the total flight time to 17.3 min accordingly.

4. Cost of design

Cost calculation is a very important task on the creation of any new product. The prize of the final product plays a significant role on the success of the product in the market. Rapid manufacturing of parts and advancements in technology have create a very competitive market where similar products can easily be created in very little time. Also, new components with enhanced capabilities can improve the performance of any designed system. For these reasons, a product which can easily be customized and upgraded holds better chances of surviving in this rapid changing market.

In order to estimate the total cost of the customized system the cost of the individual components should be calculated. Since the system is an assembly of different sub-systems it is easier to calculate the cost of each sub-system separately. By doing so the final cost of the customized drone can be altered according to the requirements of the user.

There are several methods of estimating the total cost of a product. Qualitative and quantitative analysis are the most used methods for product cost estimation [29].
Qualitative analysis includes:

1. Intuition methods which are based mostly on the knowledge of the product owner
2. Cost estimation by comparison with similar products
3. Analogical methods where the product is evaluated based in preceding similar cases.

Quantitative analysis includes:

1. Parametric cost evaluation. In this case critical components determine the final cost
2. Analytical methods, which involve all the costs occurred in the production of the product.

4.1. Cost of 3d printed components

The proposed system consists of a customized robotic arm attached to the drone frame and a selection of electronic components. The price of the electronic components is based on the price which the parts are currently available in the market. For the frame of the quadcopter and the body parts of the robotic manipulator an analytical model which includes all the direct and indirect costs occurred in the production of the part is used.

The parts needed for the construction of the quadcopter frame and the main body of the robotic manipulator have been designed with the use of Solidworks. Additive manufacturing processes like fused deposition modeling are widely used in order to produce custom made components [30] with the help of 3D printers. Such kind of printers use standard triangulation language format (STL) in order to load and prepare the designed components for 3D printing. For this project, the designed components have been loaded into the Prusa slicer software (fig. 33 and fig.34), which can simulate the printing process and also calculate all the parameters necessary for the printing of the parts.

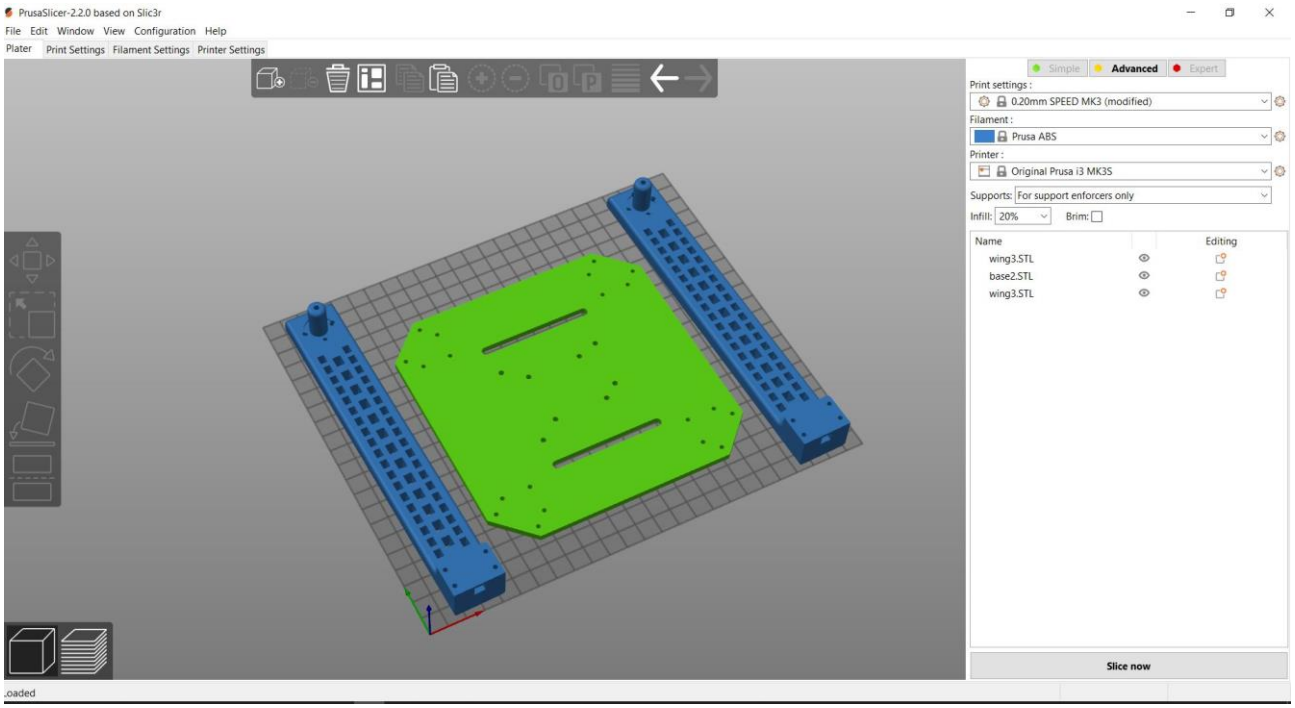

Fig. 33. Drone frame parts imported on Prusa slicer

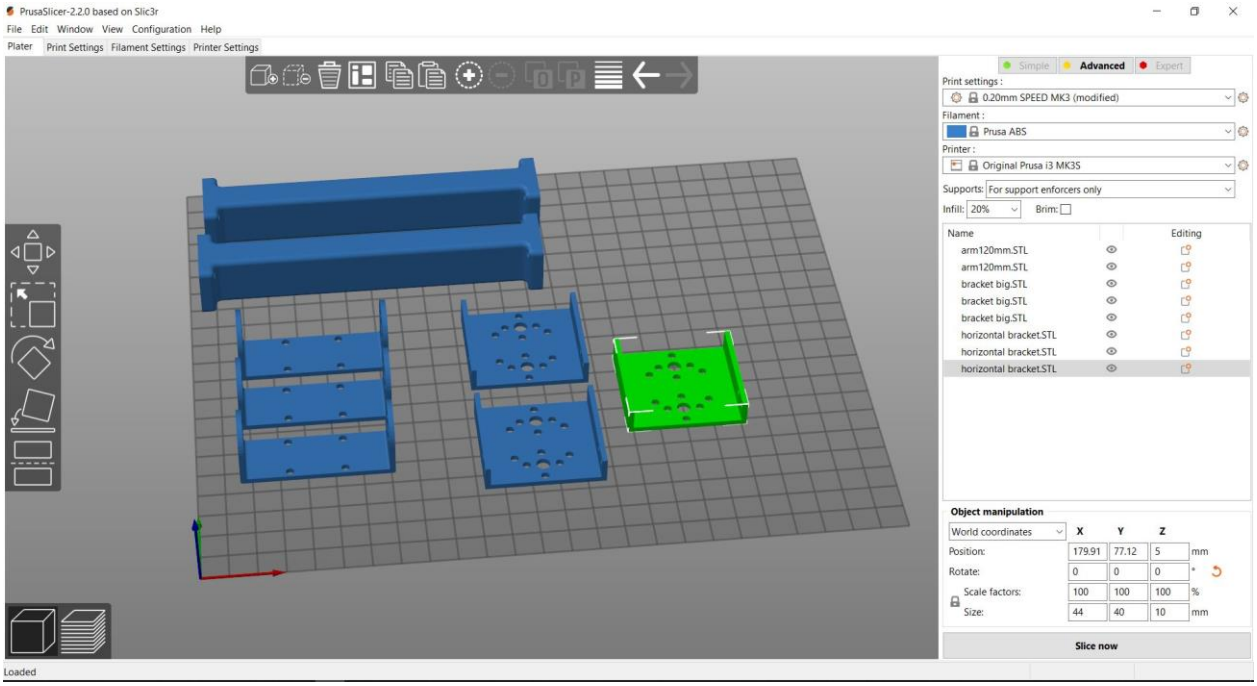

Fig. 34. Robot arm main parts imported on Prusa Slicer

The Prusa slicer software allows the user to adjust all the printing parameters in order to optimize the final print. Parameters such as the layer high, infill ration, supports and printing speed can affect the total time of printing, the material use, the cost of the part but also the mechanical characteristics of the final product [22]. For this project three different options have been considered for the printing of the components. Table 11 & 12 present the effect of changing the infill ratio to the printing parameters as calculated by the Prusa software.

Table 11. Improved drone frame parts with different infill ratios

Infill percentage	20%	50%	80%
Total filament used in meters	97.72m	122m	146m
Total filament used in grams	253.84gr	317gr	380gr
Total printing time in hours	25h	28h	32h

Table 12. Robotic manipulator attachment parts with different infill ratios

Infill percentage	20%	50%	80%
Total filament used in meters	23.29m	30.35m	37.39m
Total filament used in grams	60.5gr	78.84gr	97.14gr
Total printing time in hours	5.5h	6.5h	7h

The above data can be used in order to calculate the production costs of the 3D printed parts required for this project. The Prusa i3 MK3 3D printer was selected as the main printer with ABS filament as material. As per the manufacturer of the printer, the price of the 3D printer costs about 1000 Eur and the power consumption is about 100W. The price of 1Kg of ABS filament comes to 23 Eur. The production costs can now be calculated by [31]:

$$Total\ Production\ Cost = Consumption\ of\ material(kg) + Manufacturing\ time(h) \times MHR + Cost\ of\ Design$$

Where, material consumption is the sum of total material used multiplied by the cost per kilo of material, manufacturing time is the total printing time of the parts, and MHR stands for Machine Hourly Rate and is given by:

$$MHR(EUR/Hr) = \frac{\left(\Sigma_{depreciation} + \Sigma_{interest} + \Sigma_{occupancy\,cost} + \Sigma_{energy\,cost} + \Sigma_{maintenance\,cost} + \Sigma_{tools\,cost} + \Sigma_{employee\,cost} + \Sigma_{additional\,cost}\right)}{Machine\ Working\ Time\ \left(\frac{h}{y}\right)}$$

$$= \frac{125 + 216 + 20.5 + 1135}{2096} = 0.71\ Eur/Hr$$

where:

$$\Sigma_{depreciation} = \frac{Procurement\ value\ (Eur)}{Service\ life\ (Years)} = \frac{1000}{8} = 125\ Eur$$

$$\Sigma_{interest} = \frac{\frac{2}{3}Procurement\ value\ (Eur) \times interest\%}{100\%} = \frac{\frac{2}{3}1000}{100\%} = 666.67\ Eur$$

Cost related to interest can be omitted since the value of the 3D printer is relatively low and can be purchased without interest.

$$\Sigma_{occupancy} = Space\ cost\ rate\ \left(\frac{Eur}{Month\ m^2}\right) \times 12\ (Months) \times Required\ space(m^2) = 6 \times 12 \times 3 = 216\ Eur$$

$$\Sigma_{energy\,cost} = Machine\ maximum\ power\ (kw) \times Efficiency\ \% \times Energy\ cost\ \left(\frac{Eur}{kwh}\right) \times MWT = 0.1 \times 0.7 \times 0.14 \times 2096 = 20.5\ Eur$$

$$\Sigma_{employee\ cost} = \frac{Employee\ cost\ \left(\frac{Eur}{Hr}\right) \times MWT\ \left(\frac{Hr}{YEAR}\right)}{Printers\ per\ employee} = \frac{6.5 \times 2096}{12} = 1135\ Eur$$

$$MWT = Machine\ Working\ Hours\ per\ year \cong 262\ working\ days/y \times 8h = 2096$$

Design costs, cost related to maintenance of the 3D printer and tools cost is also omitted for simplicity reasons.

Table 13. Cost of 3D printing drone frame and robotic manipulator parts

Printer Prusa i3 MK3	**Mass of Material**	**Printing time**	**Material Price / KG**	**MHR**	**Total Material Cost**	**Part Production Cost**
Units	kg	Hr	Eur	Eur	Eur	Eur
Drone frame parts						
20% Infill	0.25	25	23	0.71	5.84	23.5
50% Infill	0.31	28	23	0.71	7.29	27.1
80% Infill	0.38	32	23	0.71	8.74	31.4
Robotic arm parts						
20% Infill	0.06	5.5	23	0.71	1.38	5.2
50% Infill	0.07	6.5	23	0.71	1.81	6.4
80% Infill	0.09	7.0	23	0.71	2.23	7.2

The cost of printing the designed parts is calculated on Table 13. Three different options have been considered. In each case adjustment of the infill ratios was done in order to calculate the final cost of each print. The consumption of material, printing speed and material cost affects the final cost of each print. Higher infill ratio value results to more solid parts. Although by increasing the infill ratio the printing time increases accordingly. However, the value of the production cost presents very small differences between each category.

4.2. Cost of electronic components

The cost of the electronic components has significantly role to the cost of the final assembly. Drone electronics are exposed to changing environmental conditions which affects the life span of the components. Accidents and crashes which may occur during flights can damage permanently the electronic components making the system non-operational. For these reasons, the lower the cost the easiest is to replace the components with new ones. The quadcopter system made for aerial thermography (Model 1), consists of components which the total cost was calculated at 490.66 Eur. For this system (Model 2) other similar parts with the same or almost the same specifications are selected. The cost of each model is compared on Table 14.

Table 14. Drone electronics comparison [14]

Part Name	Part Description	Model 1	Price in Euros	Model 2	Price in Euros	Total Savings
Drone frame	Main drone frame, 3D printed	Custom Print	12.58	Custom Print	23.5	+10.92
Motors	To provide thrust for drone	Emax 2750 kv	89.4	LHI 920KV	30	-59.4
Propellers	To attach to DC motors	5045	5	1045	5	0
ESC	Electronic speed controller to control motors speed	Tekko32 by Holybro	104	Simonk 30A	30	-64
Flight Controller	Flight controller to translate received signals and communicate to ESC for motor speed adjustments	Kakute F7 by Holybro		Elegoo Mega R3 Microcontroller	10	
Receiver	To receive control commands from ground transmitter	FrSky XM Micro by FrSky	18.45	Flysky FS-IA6B 6CH	18	-0.45
Transmitter	To control the drone	Taranis X9 Lite by FrSky	117.43	Flysky FS-16X 10CH	50	-67.43
Power Distribution Board	To divide power to all components			Matek PDB	10	+10
Video transmitter	Video transmitter to broadcast live image to ground receiver	VTX Rush Tank mini and Cherry RHCP antenna by RushFPV	64	Boscam FT952 Mini video transmitter and antenna, AV connection for action cameras	35	-29
LiPo Battery	To power up the system	LiPo Zop Power 5000mAh 4Cell	44.8	ZOP Power 11.1V 5200mAh	25	-19.8
Battery charger	To re-charge the battery	Imax B6 50W	35	Imax B6 50W	35	0
Total			490.66		271.5	-219.66

From Table 14, it was observed that even though the cost of the improved drone frame is higher than the cost of the previous compact design 23.5 vs 12.58 Eur, the total cost of model number 2 equals to 271.5 Eur which is 45% less than the cost of the components required for model 1 (490 Eur). Furthermore, the most expensive component of both model 1 and 2 is the transmitter unit, 117 Eur / 50 Eur. and the cheapest are the propellers 5 Eur. The biggest cost reduction was observed on the transmitter unit (-67.43 Eur), flight controller and speed controllers (-64 Eur), and brushless motors (-54.4 Eur). The cost related to the robotic manipulator can be calculated by summing the cost of the 3d printed parts with the cost of the four servo motors. In this case the total cost of the robotic arm equals to 71.2 Eur. The cost of the assembly (UAV Model 2 & robotic manipulator) equals to 342 Eur. However, the final cost of the system depends on the cost of the thermal camera and the additional payloads added on the drone system.

Conclusions

1. The comparison made for the previous compact frame design versus the new improved design showed sufficient results to justify the need for new improved drone frame. Under maximum load of 3kg the previous compact frame showed very large nodal stresses 22.8MPa and displacement 11.8mm, while the new improved frame presented maximum nodal stresses of 3.02 MPa and only 2.68mm displacements.

   The finite element analysis made on the improved drone frame showed good rigidity for all tested flying states and under maximum load of 3kg (Take-off max stresses 3.02 MPa. Hovering max stresses 2.78 MPa, Forward Pitch 2.77 MPa) also very small displacements were observed during each state (Take-off max displacements 2.68 MPa, Hovering max displacements 2.47 MPa, Forward Pitch 2.77 MPa).

   The results of the first and second drop test analysis showed extremely high values of nodal stresses (54.23Mpa Drop test 1 and 137.9Mpa Drop test 2) these values are way above the maximum nodal stresses limit given by the manufacturer of the ABS filament (43 Mpa). In these cases, the rigidity of the frame is compromised.
2. This research project showed that it is possible to intergrade multiple payloads into customized Unmanned Aerial Vehicles which can work in parallel with robotic manipulators in order to perform contact and contactless NDT. The robotic manipulator design made in Solidworks was validated by importing the designed system into Matlab Simulink environment where simulation of the robotic arm was made.
3. The maximum payload which the drone can carry is calculated at 3.44 kg although for safety reasons the maximum payload value was set at 2.5kg.

   The total flight time was calculated at 11.77min with maximum payload of 2.5kg. Although the current load applied on the system is 1.7kg which increases the maximum flight time to 17.3 min. Additional payload will have negative impact on the total flight time of the system. To optimize the flying time a battery with more capacity and voltage rate is required.
4. The in-fill ratio adjustments made for the 3D printed components showed very small differences in the total price of the 3D printed parts of the drone frame (20% Infill = 23,5 Eur, 50% Infill = 27,1 Eur, and 80% Infill = 31,4 Eur) while printing time between these three different setting is affected more with, 25 total hours for 20% Infill, 28h for 50% Infill and 32h for 80% Infill ratio. In case of the robotic manipulator parts, infill ratio adjustments showed very small differences in total printing time and total cost (20% Infill-5.5h printing time -5,2 Eur total cost, 50% Infill- 6.5h printing time - total cost 6,4 Eur, and 80% Infill- 7h printing time – total cost 7,2 Eur). 3D printing setting optimization is required in case of mass production of the designed components in order to justify the differences found in printing time and total cost.

   The cost of the electronic components required in order to build the new improved drone was calculated at 271.5Eur which is 45% less than the cost of the electronic components required for the compact system (490.66 Eur) made for aerial thermography only.

List of References

1. TRAMPUS, P., KRSTELJ, V. and NARDONI, G. *NDT Integrity Engineering – A New Discipline*. Procedia Structural Integrity, 2019, vol. 17. pp. 262- 267. Available from: http://dx.doi.org/10.1016/j.prostr.2019.08.035 CrossRef. ISSN 2452- 3216. DOI 10.1016/j.prostr.2019.08.035.
2. DWIVEDI, S.K., VISHWAKARMA, M. and SONI, P.A. *Advances and Researches on Non Destructive Testing: A Review*. Materials Today: Proceedings, 2018, vol. 5, no. 2, Part 1. pp. 36903698. Availablefrom: https://www.sciencedirect.com/science/article/pii/S2214785317328936 ISSN 2214-7853. DOI https://doi.org/10.1016/j.matpr.2017.11.620.
3. GHOLIZADEH, S. *A Review of Non-Destructive Testing Methods of Composite Materials*. Procedia Structural Integrity, 2016, vol. 1. pp. 50-57. Available from: http://dx.doi.org/10.1016/j.prostr.2016.02.008 CrossRef. ISSN 2452- 3216. DOI 10.1016/j.prostr.2016.02.008.
4. TSANAKAS, J.A., et al. *Fault Diagnosis and Classification of Large-Scale Photovoltaic Plants through Aerial Orthophoto Thermal Mapping* the 13th Conference on Sustainable Development of Energy, Water and Environment Systems -SDEWES2018 View Project CIRCUSOL View Project Ioannis (John) A Tsanakas Atomic Energy and Alternative Energies Commission FAULT DIAGNOSIS AND CLASSIFICATION OF LARGE-SCALE PHOTOVOLTAIC PLANTS THROUGH AERIAL ORTHOPHOTO THERMAL MAPPING. , -09, 2015.
5. OMAR, T. and NEHDI, M.L. *Remote Sensing of Concrete Bridge Decks using Unmanned Aerial Vehicle Infrared Thermography*. Automation in Construction, Nov 2017, vol. 83. pp. 360-371. Available from: http://dx.doi.org/10.1016/j.autcon.2017.06.024 CrossRef. ISSN 0926-5805. DOI 10.1016/j.autcon.2017.06.024.
6. GONZÁLEZ-DESANTOS, L.M., et al. *UAV Payload with Collision Mitigation for Contact Inspection*. Automation in Construction, 2020, vol. 115. pp. 103200. Available from: http://www.sciencedirect.com/science/article/pii/S0926580519314207 ISSN 0926-5805. DOI https://doi.org/10.1016/j.autcon.2020.103200.
7. KOCER, B.B., TJAHJOWIDODO, T., PRATAMA, M. and SEET, G.G.L. *Inspection-while-Flying: An Autonomous Contact-Based Nondestructive Test using UAV-Tools*. Automation in Construction, 2019, vol. 106. pp. 102895. Available from: http://www.sciencedirect.com/science/article/pii/S0926580519301451 ISSN 0926- 5805.DOI https://doi.org/10.1016/j.autcon.2019.102895.
8. TOGNON, M., et al. *A Truly-Redundant Aerial Manipulator System with Application to Push-and-Slide Inspection in Industrial Plants*. IEEE Robotics and Automation Letters, Apr 2019, vol. 4, no. 2. pp. 1846- 1851. Available from: https://ieeexplore.ieee.org/document/8629273 CrossRef. ISSN 2377-3766. DOI 10.1109/LRA.2019.2895880.
9. OLLERO, A., et al. The AEROARMS Project: *Aerial Robots with Advanced Manipulation Capabilities for Inspection and Maintenance*. IEEE Robotics & Automation Magazine, Dec 2018, vol. 25, no. 4. pp. 12- 23. Available from: https://ieeexplore.ieee.org/document/8435987 CrossRef. ISSN 1070- 9932. DOI 10.1109/MRA.2018.2852789.
10. RADOGLOU-GRAMMATIKIS, P., SARIGIANNIDIS, P., LAGKAS, T. and MOSCHOLIOS, I. *A Compilation of UAV Applications for Precision Agriculture*. Computer Networks (Amsterdam, Netherlands:1999), May 08, 2020, vol. 172. pp. 107148. Available from:

http://dx.doi.org/10.1016/j.comnet.2020.107148 CrossRef. ISSN 1389-1286. DOI 10.1016/j.comnet.2020.107148.

11. TAYEBI, A. and MCGILVRAY, S. *Attitude Stabilization of a VTOL Quadrotor Aircraft*. IEEE Transactions on Control Systems Technology, May 2006, vol. 14, no. 3. pp. 562-571. Available from: https://ieeexplore.ieee.org/document/1624481 CrossRef. ISSN 1063- 6536. DOI 10.1109/TCST.2006.872519.
12. HASSANALIAN, M. and ABDELKEFI, *A. Classifications, Applications, and Design Challenges of Drones: A Review*. Progress in Aerospace Sciences, May 2017, vol. 91. pp. 99-131. Available from: http://dx.doi.org/10.1016/j.paerosci.2017.04.003 CrossRef. ISSN 0376- 0421. DOI 10.1016/j.paerosci.2017.04.003.
13. LOUKAS, K. *Design of Custom-made Drone with Attached Non- Destructive Testing Equipment*. Research Project. Kaunas University of Technology, Dec 2020.
14. Banggood Global Leading Online Store [online]. [viewed Jan 2021]. Available from: https://www.banggood.com/Wholesale-RC-Quadcopter-Parts-ca-7020.html?from=nav
15. RONCORONI, M. and LANE, S.N. *A Framework for using Small Unmanned Aircraft Systems (sUASs) and SfM Photogrammetry to Detect Salmonid Redds*. Ecological Informatics, Sep 2019, vol. 53. pp. 100976. Available from: http://dx.doi.org/10.1016/j.ecoinf.2019.100976 CrossRef. ISSN 1574-9541. DOI 10.1016/j.ecoinf.2019.100976.
16. GALLARDO-SAAVEDRA, S., HERNÁNDEZ-CALLEJO, L. and DUQUE-PEREZ, O. *Technological Review of the Instrumentation used in Aerial Thermographic Inspection of Photovoltaic Plants*. Renewable & Sustainable Energy Reviews, Oct 2018, vol. 93. pp. 566-579. Available from: http://dx.doi.org/10.1016/j.rser.2018.05.027 CrossRef. ISSN 1364-0321. DOI 10.1016/j.rser.2018.05.027.
17. Flir Systems [online]. 2020.[viewed Feb 2021]. Available from: https://www.flir.eu/browse/home-amp-outdoor/drone-cameras/
18. Workswell Infrared Cameras and Systems [online]. 2020. [viewed Feb 2021]. Available from: https://workswell-thermal-camera.com/
19. Yuneen Holding [online]. 2021. [viewed Feb 2021]. Available from: https://us.yuneec.com/payloads/
20. DING, X., GUO, P., XU, K. and YU, Y. *A Review of Aerial Manipulation of Small-Scale Rotorcraft Unmanned Robotic Systems*. Chinese Journal of Aeronautics, Jan 2019, vol. 32, no. 1. pp. 200-214. Available from: http://dx.doi.org/10.1016/j.cja.2018.05.012 CrossRef. ISSN 1000-9361. DOI 10.1016/j.cja.2018.05.012.
21. Prusa Research [online]. 2021. [viewed Mar 2021]. Available from: https://shop.prusa3d.com/en/filament/130-white-easyabs-filament-1kg.html
22. BANJANIN, B., VLADIĆ, G., PÁL, M., BALOŠ, S., DRAMIĆANIN, M., RACKOV, M., KNEŢEVIĆ, I. *Consistency analysis of mechanical properties of elements produced by FDM additive manufacturing technology*. January 2018, vol.23 n.04. ISSN 1517-7076 artigo e-12250, 2018
23. HOW TO MECHATRONICS [online]. 2019. [viewed Mar 2021]. Available from: https://howtomechatronics.com/how-it-works/how-brushless-motor-and-esc-work/
24. Aerodynamics for students [online].2021. [viewed Apr 2021]. http://www.aerodynamics4students.com/propulsion/blade-element-propeller-theory.php

25. ORSAG, M., KORPELA, C., OH, P. and BOGDAN, S. *Advances in Industrial Control Aerial Manipulation*. Springer International Publishing Available from: https://explore.openaire.eu/search/publication?articleId=sygma:81af4215fd1fa0ce9be39c4d5b4682f3 DOI 10.1007/978-3-319-61022-1.
26. Brooking J. [online].2019. [viewed Apr 2021]. Available from: http://www.brokking.net/ymfc-al_main.html
27. SUAREZ, A., et al. *Design of a Lightweight Dual Arm System for Aerial Manipulation*. Mechatronics (Oxford), Apr 2018, vol. 50. pp. 30- 44. Available from: http://dx.doi.org/10.1016/j.mechatronics.2018.01.005 CrossRef. ISSN 0957-4158. DOI 10.1016/j.mechatronics.2018.01.005.
28. Omni Calculator. [online].2018. [viewed May 2021]. Available from: https://www.omnicalculator.com/
29. NANDHAKUMAR, S., et al. *Investigation of Production Costs in Manufacturing Environment using Innovative Tools*. Materials Today: Proceedings, 2020. Available from <http://www.sciencedirect.com/science/article/pii/S2214785320349063>. ISSN 2214-7853.
30. SOLOMON, I. John; SEVVEL, P.and GUNASEKARAN, J. *A Review on the various Processing Parameters in FDM*. Materials Today: Proceedings, Jun 2020. Available from <http://dx.doi.org/10.1016/j.matpr.2020.05.484> CrossRef. ISSN 2214-7853.
31. Adnan Niazi, Jian S. Dai, Stavroula Balabani, Lakmal Seneviratne, *Product cost estimation: Technique classification and methodology review* (2006): 563–575.

Appendices

Appendix 1. Technical Drawings

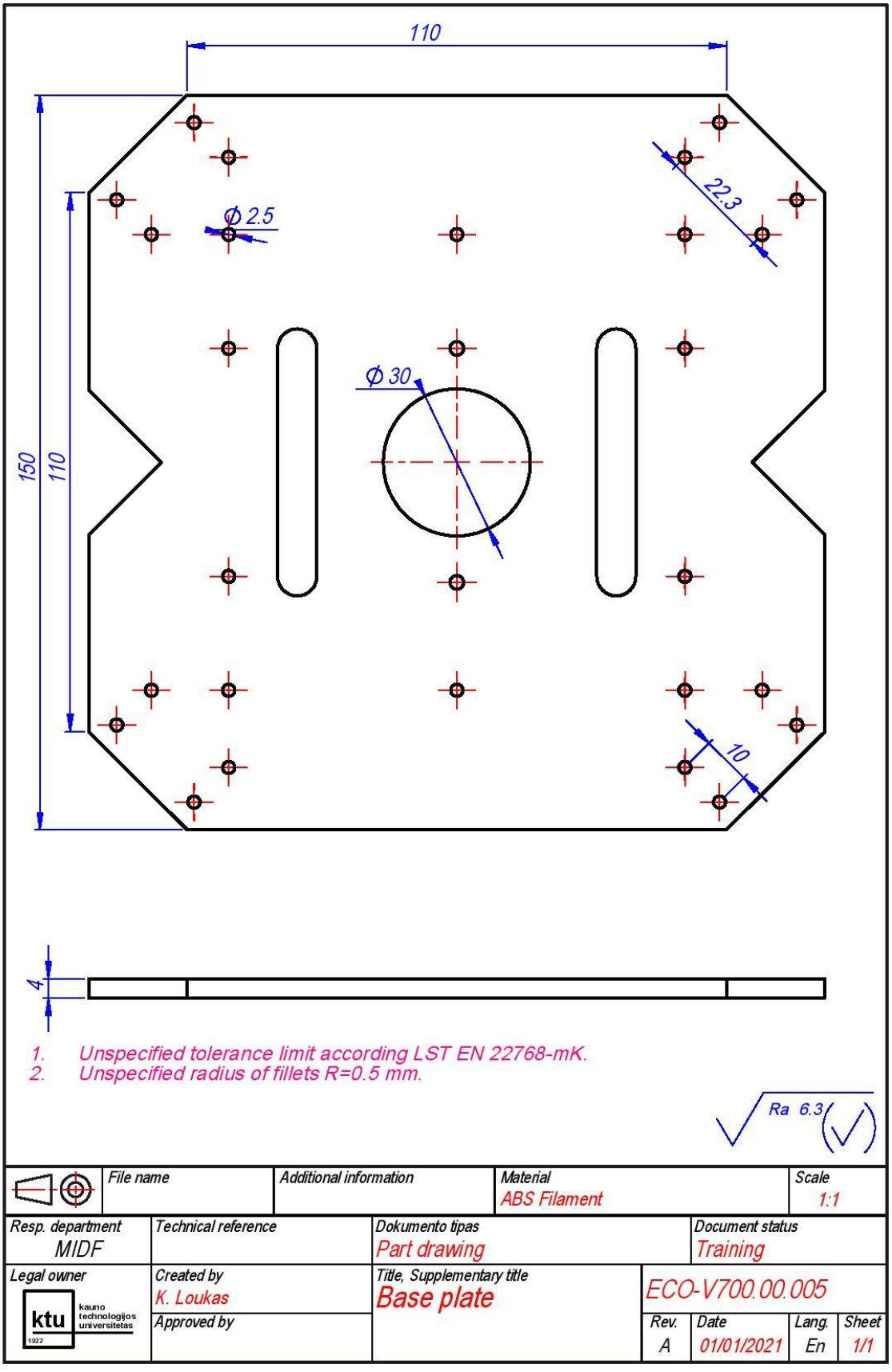

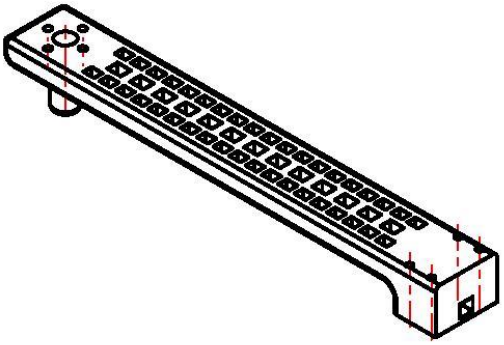

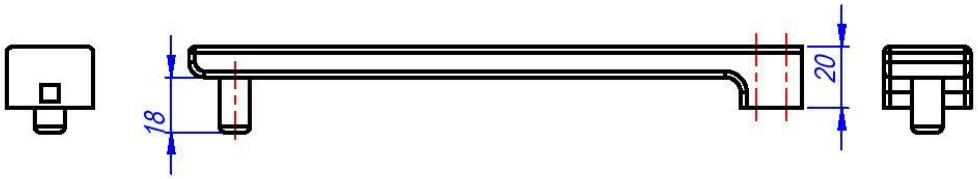

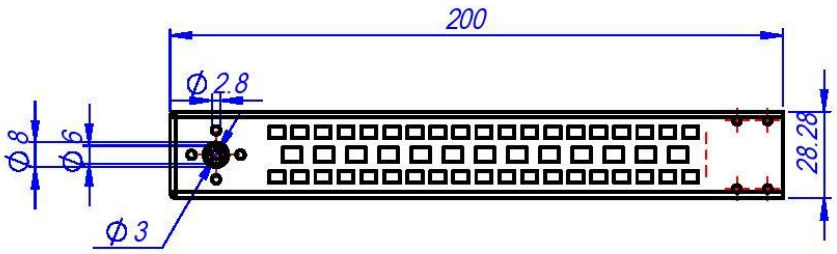

1. Unspecified tolerance limit according LST EN 22768-mK.
2. Unspecified radius of fillets R=0.5 mm.

Ra 6.3

	File name	Additional information	Material	Scale
			ABS Filament	1:2

Resp. department	Technical reference	Dokumento tipas	Document status
MIDF		Part drawing	Training

Legal owner	Created by	Title, Supplementary title	ECO-V700.00.005			
ktu kauno technologijos universitetas 1922	K. Loukas	Wing	Rev.	Date	Lang.	Sheet
	Approved by		A	01/01/2021	En	1/1

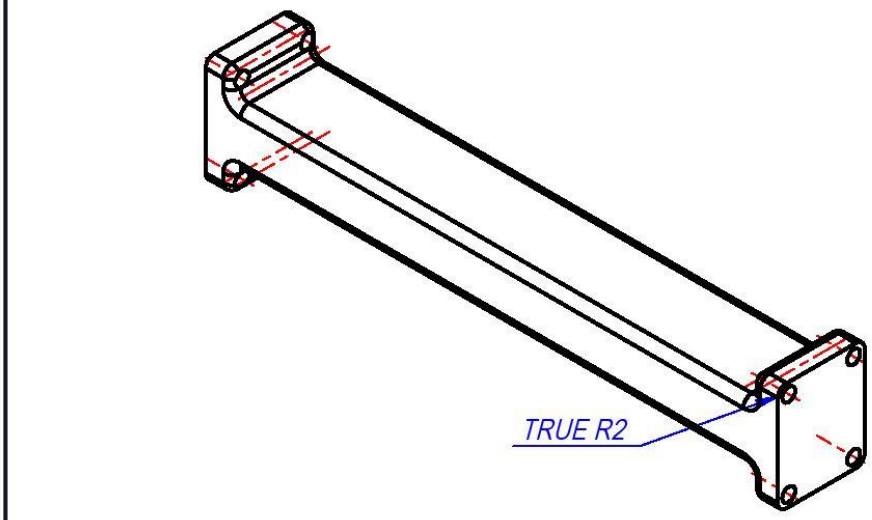

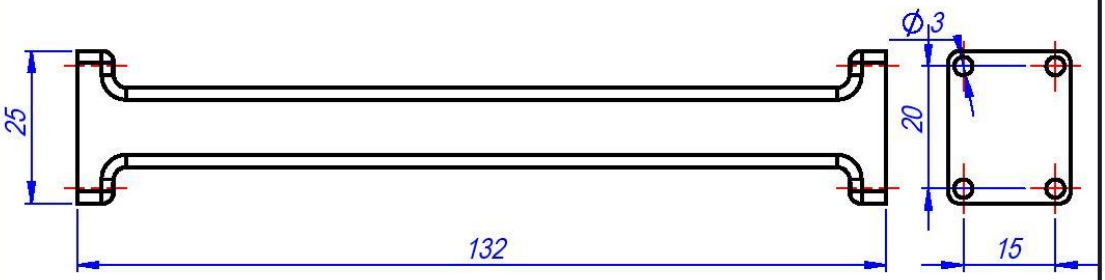

1. Unspecified tolerance limit according LST EN 22768-mK.
2. Unspecified radius of fillets R=0.5 mm.

Ra 6.3

	File name	Additional information	Material	Scale
			ABS Filament	1:1

Resp. department	Technical reference	Dokumento tipas	Document status
MIDF		Part drawing	Training

Legal owner	Created by	Title, Supplementary title	ECO-V700.00.005			
ktu kauno technologijos universitetas 1922	K. Loukas	Arm Part	Rev.	Date	Lang.	Sheet
	Approved by		A	5/14/2021	En	1/1
	Name Surname					

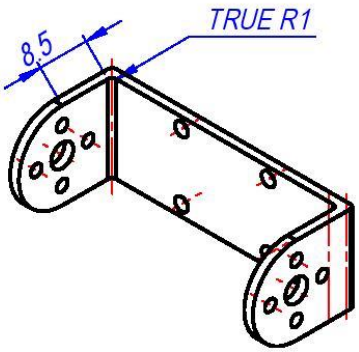

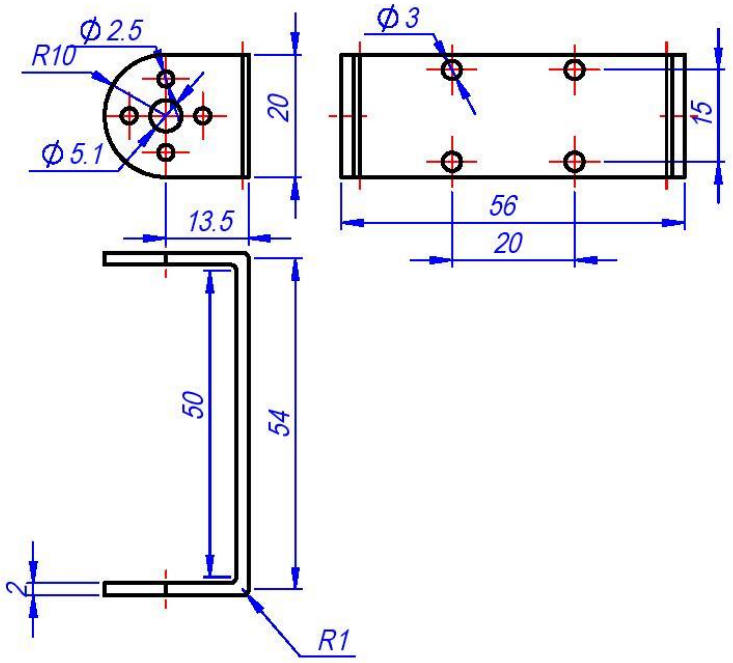

1. Unspecified tolerance limit according LST EN 22768-mK.
2. Unspecified radius of fillets R=0.5 mm.

Ra 6.3

	File name	Additional information	Material	Scale
			ABS Filament	1:1

Resp. department	Technical reference	Dokumento tipas	Document status
MIDF		Part drawing	Training

Legal owner	Created by	Title, Supplementary title	ECO-V700.00.005			
kauno technologijos universitetas	K. Loukas	Bracket Big	Rev.	Date	Lang.	Sheet
	Approved by		A	5/14/2021	En	1/1
	Name Surname					

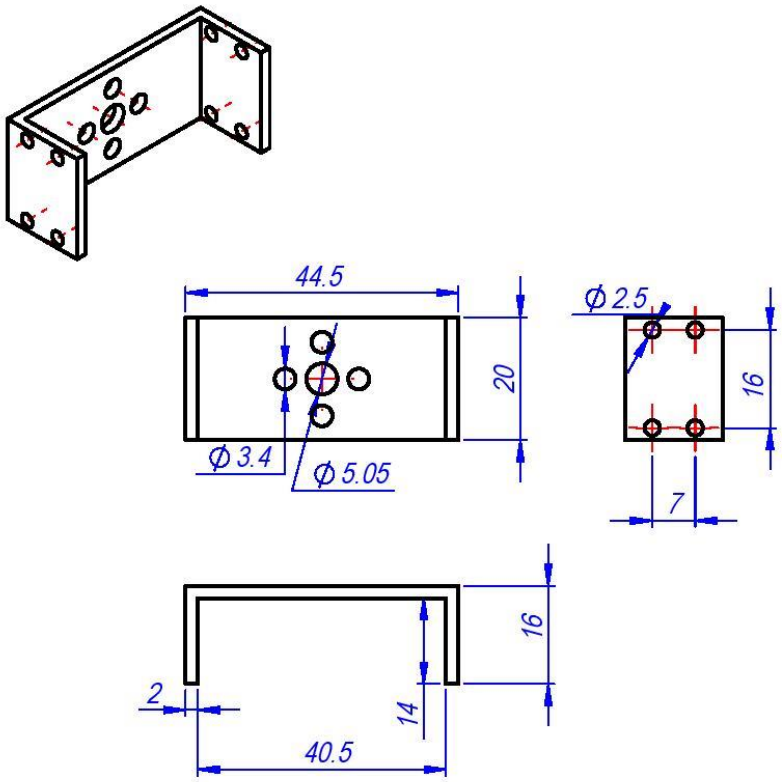

1. Unspecified tolerance limit according LST EN 22768-mK.
2. Unspecified radius of fillets R=0.5 mm.

Ra 6.3

	File name	Additional information	Material	Scale
			ABS Filament	1:1

Resp. department	Technical reference	Dokumento tipas	Document status
MIDF		Part drawing	Training

Legal owner	Created by	Title, Supplementary title	ECO-V700.00.005			
ktu kauno technologijos universitetas 1922	K. Loukas	Bracket Small	Rev.	Date	Lang.	Sheet
	Approved by		A	5/14/2021	En	1/1
	Name Surname					

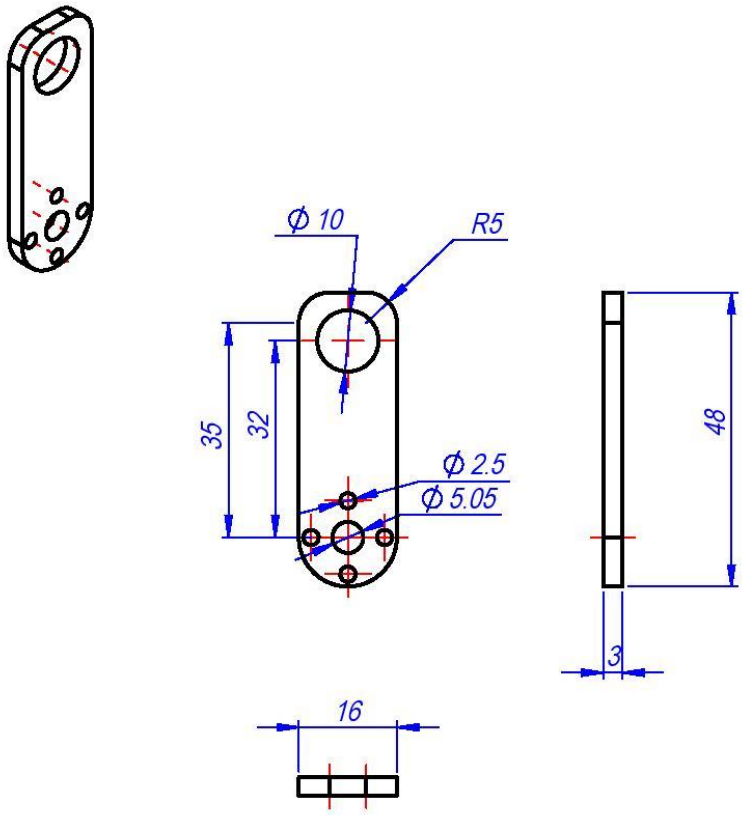

1. Unspecified tolerance limit according LST EN 22768-mK.
2. Unspecified radius of fillets R=0.5 mm.

Ra 6.3

	File name	Additional information	Material: ABS Filament	Scale: 1:1
Resp. department: MIDF	Technical reference	Dokumento tipas: Part drawing		Document status: Training
Legal owner: kauno technologijos universitetas (ktu, 1922)	Created by: K. Loukas	Title, Supplementary title: Probe Holder	ECO-V700.00.005	
	Approved by: Name Surname		Rev.: A	Date: 5/14/2021 / Lang.: En / Sheet: 1/1

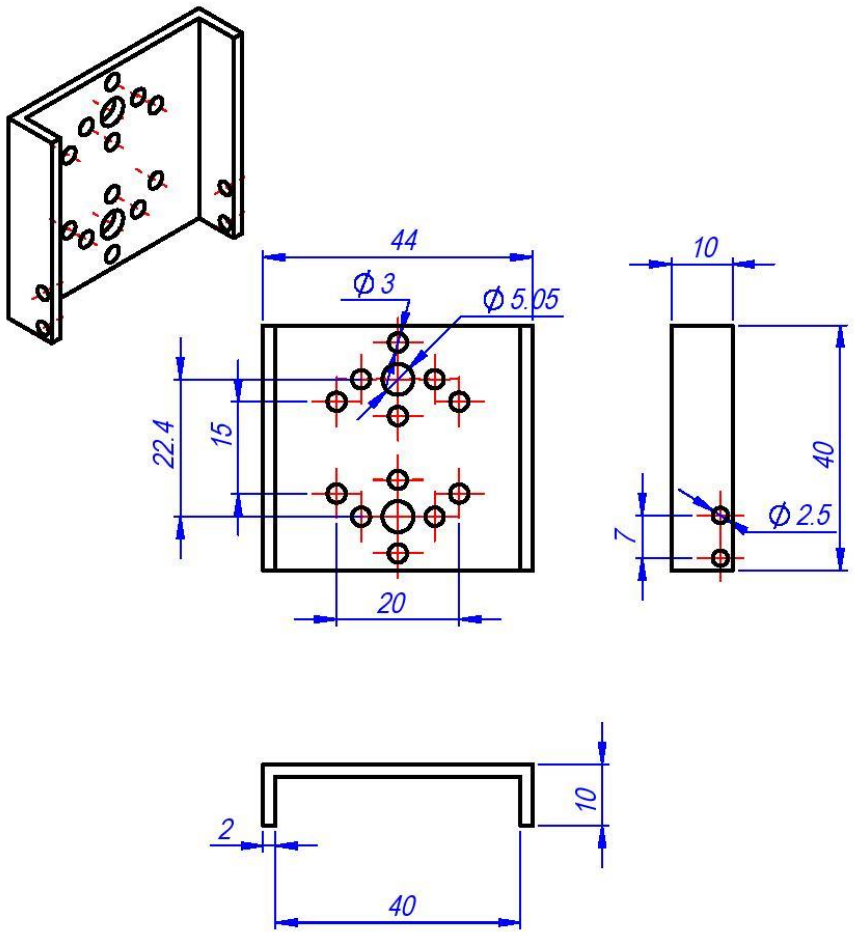

1. Unspecified tolerance limit according LST EN 22768-mK.
2. Unspecified radius of fillets R=0.5 mm.

Ra 6.3

	File name	Additional information	Material	Scale
			ABS Filament	1:1

Resp. department	Technical reference	Dokumento tipas	Document status
MIDF		Part drawing	Training

Legal owner	Created by	Title, Supplementary title	ECO-V700.00.005			
ktu kauno technologijos universitetas 1922	K. Loukas	Servo Holder	Rev.	Date	Lang.	Sheet
	Approved by		A	5/14/2021	En	1/1
	Name Surname					

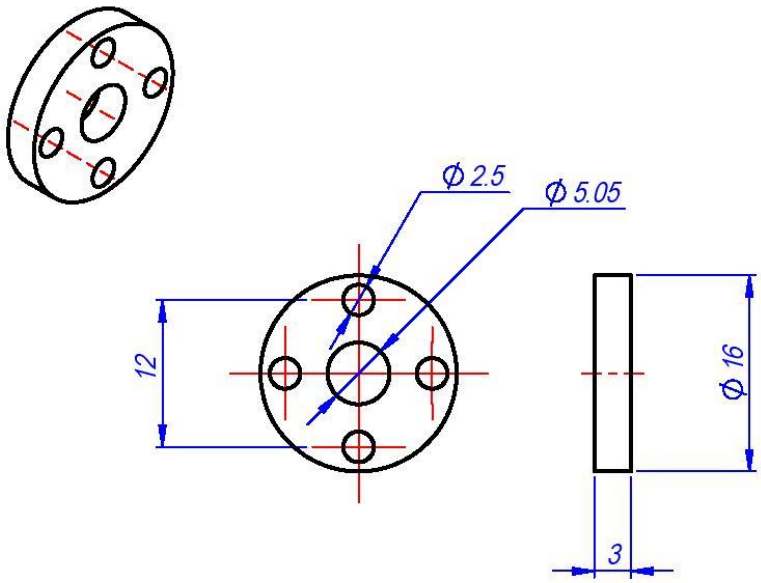

1. Unspecified tolerance limit according LST EN 22768-mK.
2. Unspecified radius of fillets R=0.5 mm.

Ra 6.3

File name	Additional information	Material	Scale
		ABS Filament	1:1

Resp. department	Technical reference	Dokumento tipas	Document status
MIDF		Part drawing	Training

Legal owner	Created by	Title, Supplementary title	ECO-V700.00.005			
kauno technologijos universitetas	K. Loukas	Servo Pulley	Rev.	Date	Lang.	Sheet
	Approved by		A	5/14/2021	En	1/1
	Name Surname					